Universidade de Aveiro 2017

Departamento de Ambiente e Ordenamento (DAO)

Rui Gonçalves Pinto

Síntese de faialite (Fe_2SiO_4) para catalisadores de conversão de alcatrões na gasificação de biomassa

Universidade de Aveiro 2017

Departamento de Ambiente e Ordenamento (DAO)

Rui Gonçalves Pinto

Synthesis of Fayalite Fe_2SiO_4 as a Tar Removal Catalyst for Biomass Gasification

Dissertação apresentada à Universidade de Aveiro para cumprimento dos requisitos necessários à obtenção do grau de Mestre em Sistemas Energéticos Sustentáveis, realizada sob a orientação científica do Doutor Luís António da Cruz Tarelho, professor auxiliar do Departamento de Ambiente e Ordenamento da Universidade de Aveiro e do Doutor Jorge Ribeiro Frade, professor catedrático do Departamento de Engenharia de Materiais e Cerâmica, da Universidade de Aveiro

This work was supported by project LEANCOMB (refs. PTDC/CTM-ENE/2942/2014 and 04/SAICT/2015), financed by COMPETE 2020 Programme and National Funds through the FCT/MEC and when applicable co-financed by FEDER under the PT2020 Partnership Agreement.

Dedico este trabalho à minha família:

aos meus pais por todo o apoio que me deram, sem eles nunca teria sido possível;

ao meu irmão Roberto pela força;

a minha Avó pela força de vontade dela e caracter, e finalmente ao mais recente membro da família, a Ema.

O júri

Presidente	Professor Doutor António Gil D'orey de Andrade Campos Professor auxiliar do departamento de engenharia mecânica da Universidade de Aveiro
Vogais	Professor Doutor Luís António da Cruz Tarelho (Orientador) Professor auxiliar do departamento de ambiente e ordenamento da Universidade de Aveiro
	Doutor Andrei Kovalevsky (Arguente) Equiparado a investigador principal do departamento de engenharia de materiais e cerâmica da Universidade de Aveiro

Agradecimentos

As primeiras palavras de agradecimento vão para os supervisores desta tese, Professor Doutor Luís Tarellho (orientador) e o Professor Doutor Jorge Frade (co-orientador), que propuseram o presente trabalho. Deles recebi amizade, sugestões e disponibilidade, que tornaram menos árida e mais aliciante a sua elaboração.

Quero agradecer ao Doutor Aleksey Yaremchenko, por toda a ajuda, disponibilidade e ensinamentos prestados na componente laboratorial.

Aos meus colegas do 9-2-9, companheiros de laboratório e de noitadas, pela sua amizade, pelos bons momentos que partilhámos, e pelos ensinamentos e sugestões dadas, tanto no laboratório como para a escrita do documento.

Ao Mestre Daniel Pio e Licenciado João, um agradecimento por tornarem possível os ensaios na gasificação.

Um agradecimento à Mestre Daniela Lopes (9-2-9), pela ajuda prestada no meu Inglês.

Quero também dirigir uma palavra de apreço aos meus familiares, minha namorada Daniela e amigos mais próximos que, durante este trabalho, souberam compreender as minhas prolongadas ausências e os meus horários pouco ortodoxos.

A todos um sincero
MUITO OBRIGADO!

Palavras-chave: Biomassa, gasificação, alcatrões, catalisador, gás de síntese

Resumo: A formação de alcatrões é um dos principais problemas durante a gasificação de biomassa. Neste contexto têm sido propostos diferentes catalisadores para promover a eliminação destes compostos, incluindo a sua reformação com ênfase em catalisadores à base de Ni-(Ni/Al_2O_3, $Ni/MgAl_2O_4$) e minerais de baixo custo, tais como olivinas, $(Fe,Mg)_2SiO_4$. No entanto, os mecanismos e fatores de influência (efeito de composição, pré-tratamentos térmicos e seus efeitos estruturais e microestruturais) ainda são pouco compreendidos.

O presente trabalho está focado no desenvolvimento de um procedimento para a preparação da faialite sintética Fe_2SiO_4, com posterior aplicação em processos de gasificação com o objetivo de melhorar a qualidade do gás produzido em resultado da destruição de alcatrões

A faialite foi sintetizada com a mistura de Fe_2O_3 + SiC, com estequiometria 1:1, em atmosfera de CO_2 com temperatura de 1100 ºC.

A faialite demonstrou o seu poder catalítico, nas experiências de gasificação de biomassa realizadas, tendo-se verificado a eliminação de alcatrões e a redução dos gases oxidados (CO_2 e H_2O), e um enriquecimento do gás produto em CO e H_2.

Keyword: Biomass, gasification, tar, catalyst, syngas

Abstract: The formation of tars is one of the main problems during the gasification of biomass. In this context, different catalysts have been proposed to promote the elimination of these compounds, including their reforming with emphasis on catalysts based on Ni (Ni/Al_2O_3, $Ni/MgAl_2O_4$), low cost minerals such as olivines $(Fe,Mg)_2SiO_4$. However, the mechanisms and influence factors (composition effect, thermal pretreatment and its structural and microstructural effects) are still poorly understood.

The present work is focused on the development of a procedure for preparation of synthetic fayalite Fe_2SiO_4, the iron-rich end -member of the olivine solid-solution series, with intention of subsequent catalytic studies of conversion of tar, resulting from biomass gasification, in a pilot scale reactor. Fayalite was synthesized with mixture of Fe_2O_3 + SiC with stoichiometric 1:1, in atmosphere of CO_2 with temperature of 1100 ºC. Fayalite demonstrated its catalytic activity in the biomass gasification experiments carried out, occurring elimination of tars and reduction of oxidized gases (CO_2 and H_2O), and the enrichment of the product gas in CO and H_2

Index

Tables

Figures

List of abbreviations

BFB	Bubbling Fluidized Bed
CRT	Cathode Ray Tube
EDP	Energias de Portugal
EDS	Energy dispersive spectroscopy
EU	European Union
GC	Gas Chromatography
LHV	Lower Heating Value
SEM	Scanning electron microscopy
TGA	Thermogravimetric analysis
XRD	x-ray diffraction

List of symbols

$CaMg(CO_3)_2$	Dolomite
CaO	Calcium oxide
D	Distance between lattice planes
$FeC_2O_4*2H_2O$	Iron(II) oxalate dihydrate
$Fe(NO_3)_3*9H_2O$	Iron(III) nitrate nonahydrate
Fe_2O_3	Hematite
Fe_2SiO_4	Fayalite
MgO	Magnesium oxide
Mg_2SiO_4	Forsterite
SiC	Silican Carbide
λ	Wavelenght
θ	Diffraction angle

I. Introduction

1.1 Preamble

A sustainable energy future requires the combination of renewable and advanced energy technologies. Biomass is gaining attention nowadays as one of the potential sources of renewable energy. Different biomass conversion processes produce heat, electricity and fuels. Gasification is one of the most promising biomass conversion processes [1], as discussed in section 1.6.

The term biomass covers the raw (wood, energy crops and agricultural residues) or processed organic matter (effluents, food processing residues and green wastes) which can either be of vegetal or animal origin. Depending strongly on its origins, biomass materials are generally composed of cellulose, hemicellulose, lignin, lipids, proteins, simple sugar and starches [2].

Biomass can only be considered as a clean and renewable energy if obtained in a sustainable way. If the CO_2 emission from thermochemical conversion of biomass is not compensated by the natural growth of biomass and atmospheric CO_2 uptake by biomass, the biomass cannot and must not be considered as a clean and renewable energy. The term "bioenergies" refers to all the processes (industrial or not) which can convert energy from biomass [2].

Most of the biomass is used for "traditional use". i.e., heating or cooking (9%). Despite the fact that the useful energy production from biomass becomes more interesting in or developing countries, its actual share in the total global energy consumption is still very low (≈3.3%) [2].

Tar is a mixture of condensable aromatic compounds, and its formation is one of the major problems to deal with during biomass gasification due to several issues associated with condensation, formation of tar aerosols and polymerization to form more complex structures, which cause problems in the process equipment [1].

Tar can condense or polymerize into more complex structures in gas ducts, heat exchangers or in particulate filters decreasing the total efficiency and, consequently, increasing the cost of the process. Tar elimination from the product syngas is necessary before using the gas in any application [3].

Tar removal technologies can be divided into two approaches: hot gas cleaning after the gasifier (secondary methods) and treatments inside of the gasifier (primary methods). The secondary methods include tar cracking, either thermally or catalytically; or mechanical separation using cyclones, filters or scrubbers. Although these methods have proven to be effective, treatments inside the gasifier are gaining more attention as they may eliminate the need for downstream cleanup. The different approaches of primary treatment include a proper selection of operational parameters, the use of bed additive catalyst and gasifier modifications [3].

For both secondary and primary methods, the catalytic steam reforming process is a very attractive technique for destruction of tar [3].

1.2 Renewable energy

Energy sources can be divided into their main categories: fossil fuels, nuclear resources and renewable energy sources. The renewable energy sources has the ability to provide energy free of air pollutants and greenhouse gasses by emitting zero or nearly zero percent of these gases. Currently, renewable energy sources supply about 24% of the total world energy demand, which was only 2% in 1998 including 7 EJ of modern biomass and 2 EJ of all other renewable sources (1 EJ=10^{18} J). Some of the renewable energy technologies (hydropower, wind energy, solar energy, biomass energy) became mainstream and contribute towards the safety of the planet earth and its living creatures. Apart from these mainstream renewable technologies, there are some new renewable energy technologies, which are sustainable for countering the greenhouse gasses and air pollution risks to the earth [4].

At present, more mature and reliable renewable energies are on the rise and compete with the conventional energy sources. Shore wind, solar, concentrated solar, geothermal, marine energy and bio-energy are on track, and in some circumstances, they have overcome the economic constraints. The share of renewable energy sources in the global final energy consumption is increasing [4].

In 2012, renewable energy provided an estimated 19% of the global energy consumption, and it increased to 24% in 2014. The year 2015 has the largest global capacity additions seen to date. It was been observed that among various renewable energy sources, the hydropower share is on the top at 17% of the total 23%, while the wind, bio-power, and solar power shares are 3.7%, 2.0% and 1.2% respectively. Other renewable energy sources, such as concentrated solar photovoltaic, marine geothermal and others contribute only 0.4% [4].

1.3 Types of renewable energy

Renewable energy sources cover solar thermal and photovoltaic energy, hydro (including tide, wave and ocean energy), wind, geothermal energy and all forms of biomass (including biological waste and liquid biofuels). The renewable energy delivered to final consumers (industry, transport, households, services including public service, agriculture, forestry and fisheries) is the numerator of this indicator. The denominator, the gross final energy consumption of all energy sources, covers total energy delivered for energy purposes to final consumers as well as the transmission and distribution losses for electricity and heat. It should be noted that exports/imports of electricity are not considered as renewable energy unless a specific intergovernmental agreement has been signed [5].

1.4 Renewable energy in Europe and in Portugal

Since the publication of the Kyoto Protocol, which established targets for the reduction of greenhouse gases emissions, many countries and regions, including European Union, have promoted the use of renewable energy sources [6].

The energy policy in the European Union (EU) is strongly driven by the twin objectives of sustainability (including environmental aspects) and security of supply. Implementation of environmentally friendly energy options, such as renewable energy sources is key means of satisfying these objectives [7].

In 2010, energy from renewable sources was estimated to have contributed 12.4% of gross final energy consumption in the EU27, compared with 11.5% in 2009 and 10.5% in 2008. The 2009 directive on renewable energy set individual targets for all Member States, such that the EU will reach a 20% share of total energy consumption from renewable sources by 2020 [8].

Table 1: Share (in %) of renewable energy source on of gross final energy consumption (adapted) [5].

geo\time	2004	2012	2013	2014	2015	TARGET
EU (28 countries)	8.5	14.4	15.2	16.1	16.7	20
Belgium	1.9	7.2	7.5	8	7.9	13
Bulgaria	9.4	16	19	18	18.2	16
Czech Republic	6.8	12.8	13.8	15.1	15.1	13
Denmark	14.9	25.7	27.4	29.3	30.8	30
Germany	5.8	12.1	12.4	13.8	14.6	18
Estonia	18.4	25.8	25.6	26.3	28.6	25
Ireland	2.4	7.2	7.7	8.7	9.2	16
Greece	6.9	13.5	15	15.3	15.4	18
Spain	8.3	14.3	15.3	16.1	16.2	20
France	9.4	13.4	14.1	14.7	15.2	23
Croatia	23.5	26.8	28	27.9	29	20
Italy	6.3	15.4	16.7	17.1	17.5	17
Cyprus	3.1	6.8	8.1	8.9	9.4	13
Latvia	32.8	35.7	37.1	38.7	37.6	40
Lithuania	17.2	21.4	22.7	23.6	25.8	23
Luxembourg	0.9	3.1	3.5	4.5	5	11
Hungary	4.4	15.5	16.2	14.6	14.5	13
Malta	0.1	2.8	3.7	4.7	5	10
Netherlands	2.1	4.7	4.8	5.5	5.8	14
Austria	22.6	31.4	32.3	32.8	33	34
Poland	6.9	10.9	11.4	11.5	11.8	15
Portugal	**19.2**	**24.6**	**25.7**	**27**	**28**	**31**
Romania	16.3	22.8	23.9	24.8	24.8	24
Slovenia	16.1	20.8	22.4	21.5	22	25
Slovakia	6.4	10.4	10.1	11.7	12.9	14
Finland	29.2	34.4	36.7	38.7	39.3	38
Sweden	38.7	51.1	52	52.5	53.9	49
United Kingdom	1.1	4.6	5.7	7.1	8.2	15

Between 2006 and 2010, all member States increased their share of renewable energy in total consumption. The largest increases were recorded in Estonia (from 16.1% in 2006 to 24.3% in 2010), Romania (from 17.1% to 23.4%), Denmark (from 16.5% to 22.2%), Sweden (from 42.7% to47.9%) and Spain (from 9.0% to 13.8%) [8].

Energy from renewable sources was estimated to have contribute 14.1% of gross final energy consumption in 2012 in the EU28 [9], 15.0% in 2013 [10], and 16.7% in 2015 [5], as compared with 8.3% in 2004, the first year for which the data is available, [6], [9], [10]. Portugal is one of the leading countries in EU in terms of renewable energy generation and covered 28% of its energy demands using renewable energy sources (Table 1).

The share of renewables in gross final consumption of energy is one of the headline indicators of the Europe 2020 strategy. The target to be reached by 2020 for the EU is share of 20% energy from renewable sources in gross final consumption of energy. However, renewables will continue to play a key role in helping the EU meet its energy needs beyond 2020. For this reason, Member States have already agreed on a new EU renewable energy target of at least 27% by 2030 [5].

1.5 Biomass as renewable energy source

Biomass is all the organic material that comes from plants including algae, trees and crops, being derived from the reaction between CO_2 in the air, water and sunlight through photosynthesis, in order to produce carbohydrates that form the biomass [4]. It is produced by plants and includes all land and water-based vegetation, as well as all organic wastes. The biomass resource can be considered as organic matter, in which the energy of sunlight is stored in chemical bonds [11].

Biomass has always been a major source of energy for mankind and it is presently estimated to contribute around 10-14% of the energy supply of the world [11].

Researchers characterise the various types of biomass in different ways, but one simple method is to define four main types, namely, woody plants, herbaceous plants/grasses, aquatic plants, and manures [11].

The main material properties of interest during consequent processing as an energy source are moisture content, calorific value, proportions of fixed carbon and volatiles, ash/residue content, alkali metal content and cellulose/lignin ratio. For dry biomass conversion processes, the first five properties are more relevant, while for wet biomass conversion processes, the most important are the first and last properties [11].

Different technological processes can be used to obtain the various energy products from biomass. The choice of the best technology is influenced by several issues, such as the biomass kind, the preferred energy (electricity, thermal energy or boiler fuel), as well as environmental and economic issues. Energy production techniques are generally classified into two main groups: bio-chemical and thermo-chemical processes. The different biomass conversion options are shown in Fig.1.

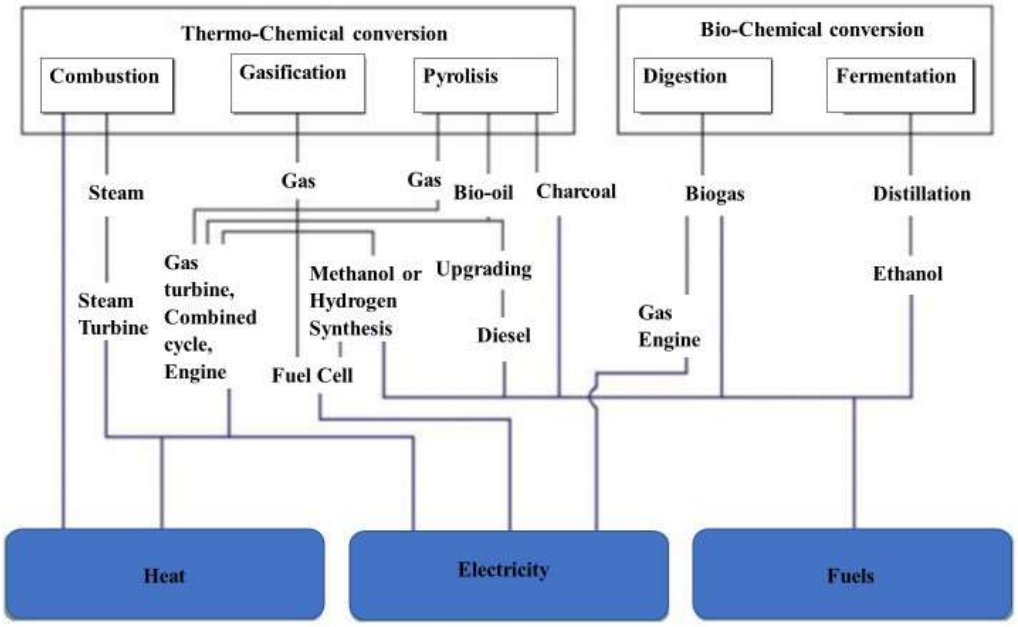

Fig. 1: Different biomass conversion technologies and their products (adapted) [12].

In Portugal biomass is defined by Decree-Law no. 127/2013 as the set of products consisting in whole or in part of vegetable matter derived from agriculture or forestry, which can be used as fuel for the purpose of recovering its energy content, as well as certain forms of waste when used as fuel, [6].

Until 2005, only two biomass power plants existed in Portugal that used biomass as a fuel: EDP in Mortágua and Centroliva in Vila Velha de Ródão. Between 2007 and 2009, five new power stations were established with a combined power of 78 MW, meaning that the total power produced from forest biomass is now more than 100 MW, [6].

1.6 Biomass gasification

Biomass is carbon based and is composed of a mixture of organic molecules containing hydrogen, usually including atoms of oxygen, often nitrogen and small quantities of other atoms, including silica, alkaline earth and heavy metals [13].

Thermochemical processes including combustion, pyrolysis and gasification (Fig.1) can convert biomass into the useful bio-energy and bio-char. Biomass pyrolysis or gasification is recognized as one of the most promising technologies for producing sustainable fuels that could be used for power generation systems or syngas applications. Biomass pyrolysis at relatively higher temperatures could produce the bio-char, bio-oil and syngas for boiler and power generation [13].

The thermochemical processes are generally more efficient than the biochemical ones for the following reasons: (1) a lower reaction time (a few seconds or minutes for thermochemical processes vs several days, weeks or even longer for biochemical/biological processes); (2) a higher ability to destroy most of the organic compounds. Lignin material is typically considered to be nonfermentable and thus cannot be completely

decomposed with biological processes, where it can be fully converted due to thermochemical transformations. In comparison to fossil fuels, biomass has lower heating values on a similar weight basis. In fact, the heating value of biomass ranges from 15 to 19 GJ/t compared to 20-30 GJ/t for coals. In comparison to fossil fuels, biomass also contains much higher volatile matter contents (80% in biomass instead of 20% for fossil fuels), which means that biomass has a high ignition stability and can easily be thermochemically processed toward other higher value fuels (syngas) [2].

Gasification of biomass has several environmental merits over fossil fuels, namely lower emission of CO_2 and other flue gases, such as H_2S, SO_2, NO_X. Biomass gasification is a thermochemical process in which biomass undergoes the incomplete combustion to yield a gas product referred to syngas that mainly consists of H_2, CO, CH_4, CO_2, and N_2 (if air or N_2 is used as the carrier gas) in various proportions. Gasification has considerable advantages compared to the direct combustion as it can convert the low-value feedstocks to high quality liquid fuels [13].

Processes occurring in biomass gasification are often distinguished into drying and devolatilization, volatile and char combustion, gasification, tar reforming with steam and CO_2 [13].

Gasification reaction occurs at temperatures between 800 and 1200°C; several parallel gasification reactions take place inside the gasifier (Table 2). The produced tars may be converted by further partial oxidation or a combination of reforming, hydrogenation, and thermal cracking, with highly endothermic reaction enthalpies between 200 and 300 kJ/mol (Nos. 1-5). The char and volatile compounds (CO, H_2 and CH_4) combustion via partial or complete oxidation reactions occurs in the presence of air or oxygen (Nos. 6,7,13-16). These reactions are highly exothermic and allow generation of the necessary heat for the drying, pyrolysis, and gasification reactions. The produced H_2O and CO_2 are thereafter consumed during the char gasification (Nos. 8-12). Reaction of water-gas shift (No. 17) and methanation (Nos. 18,19) take place in either direction, depending on the specific temperature, pressure, and reactants' concentrations. Water-gas shift is of great importance since it plays a significant role for the generation of hydrogen, and therefore for the LHV of the syngas. The methanation reactions occur slowly at low temperatures and in the absence of any catalysts. The Gibb's energy for the Boudouard (No. 8) and water-gas shift (No. 17) reactions are negative at temperatures above 720 °C and up to 820 °C [2].

Table 2: Main reactions involved in the biomass gasification process (adapted) [2].

	Heat of reaction ($kJ.mol^{-1}$) at 298 K	Reactions Name	Reaction Number
Tars general equations			
$C_nH_m+\frac{n}{2}O_2\rightarrow nCO+\frac{m}{2}H_2$		Tars partial oxidation	1
$C_nH_m+nCO_2\rightarrow 2nCO+\frac{m}{2}H_2$		Tars dry reforming	2
$C_nH_m+nH_2O\rightarrow 2CO+\left(\frac{m}{2}+n\right)H_2$	Higly endothermic +(200-300)	Tars steam reforming	3
$C_nH_m+\left(2n-\frac{m}{2}\right)H_2\rightarrow nCH_4$		Tars hydrogenation	4
$C_nH_m\rightarrow\left(n-\frac{m}{2}\right)C+\frac{m}{4}CH_4$		Tars thermal cracking	5
Char combustion			
$C+O_2\rightarrow CO_2$	-394	Complete combustion	6
$C+\frac{1}{2}O_2\rightarrow CO$	-111	Partial combustion	7
Char gasification			
$C+CO_2\rightarrow 2CO$	+172	Boundouard reaction	8
$C+H_2O\rightarrow CH_4+CO_2$	+136	Water-gas reaction 1	9
$2C+H_2O\rightarrow CH_4+CO_2$	+11	Water-gas reaction 2	10
$C+2H_2O\rightarrow CO_2+2H_2$	+103	Water-gas reaction 3	11
$C+2H_2\rightarrow 2CH_4$	-87	Hydrogasification reaction	12
Homogeneous volatile oxidation			
$CO+\frac{1}{2}O_2\rightarrow CO_2$	-283	Carbon monoxide combustion	13
$H_2+\frac{1}{2}O_2\rightarrow H_2O$	-242	Hydrogen combustion	14
$CH_4+2O_2\rightarrow CO_2+2H_2O$	-800	Methane combustion	15
$CH_4+\frac{1}{2}O_2\rightarrow CO+2H_2$	-23	Methane partial combustion	16
$CO+H_2O\rightarrow CO_2+H_2$	-37	Water-gas shift reaction	17
Methanation reactions			
$CO+3H_2\rightarrow CH_4+H_2O$	-223	Methanation reaction 1	18
$2CO+2H_2\rightarrow CH_4+CO_2$	-260	Methanation reaction 2	19

1.7 Tars from biomass gasification

Condensable aromatic organics referred to as "tar" are generated with the producer gas during biomass gasification, and their contents vary from 0.5-100 g/m^3 mainly depending on the design of a gasifier, feedstock types and operating conditions. Tar is a generic term comprising all organic compounds in syngas except for gaseous hydrocarbons, and it can condense or polymerize to more complex structures in pipes, filters, or heat exchangers of downstream equipment and processes, which may result in the mechanical breakdown of the entire system. Additionally, tars may deactivate catalysts in the refining process. In order to commercialize this technology for future applications in power generation and synthetic fuel production, the removal of tar should be considered by adsorption and reforming to syngas [13].

Tar can be classified by solubility and condensability into five classes (Table 3). Class 1 refers to the heaviest tars undetectable by Gas Chromatography (GC), which can condense at high temperatures and very low concentrations; class 2 refers to the heterocyclic aromatic compounds with water solubility (phenol and cresol); class 3 refers to the light single-ring aromatic compounds (toluene and xylene); class 4 refers to the light poly-aromatic hydrocarbons (2-3 rings), which can condense at relatively high concentration and intermediate temperatures (indene and naphthalene); at last, class 5 refers to the heavy poly-aromatic hydrocarbons (4-7 rings), condensing at high temperatures and low concentration (pyrene and coronene) [13].

Biomass tar (Fig. 2) is a complex organic mixture of the condensable or non-condensable hydrocarbons comprising 1 to 5 rings compounds along with other oxygen-containing hydrocarbons and polycyclic aromatic hydrocarbons produced during the thermochemical conversion [1], [13]. It is challenging to understand the catalytic decomposition behaviour of the real biomass tar, due to the wide range of different compounds present in tar [1].

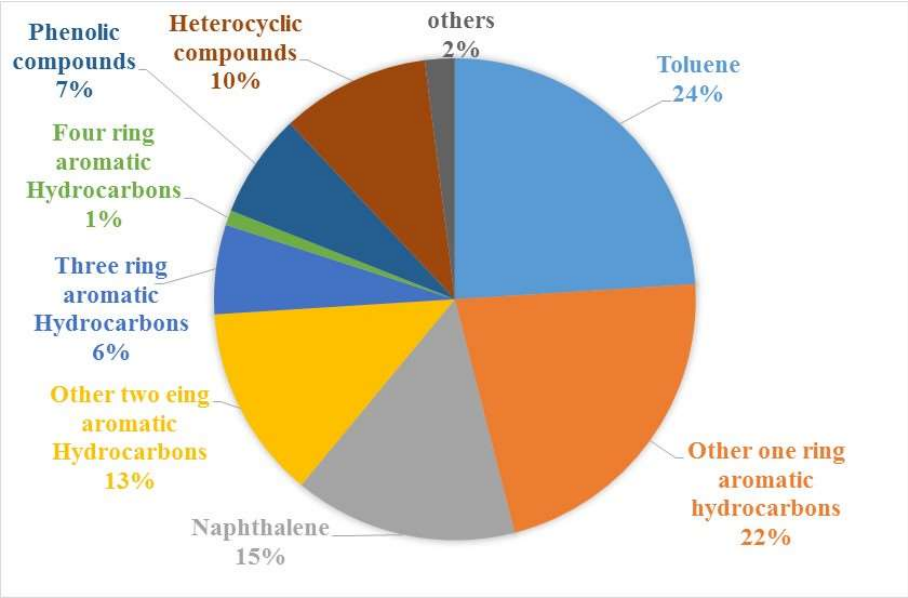

Fig. 2: Tars in raw gas during biomass gasification (adapted) [14].

Table 3: List of tar compounds that are considered for different tar classes (adapted) [15].

Tar class	Class name	Property	Representative compounds
1	GC undetectable Heterocyclic	Very heavy tars, cannot be detected by GC	None
2	Heterocyclic	Tars containing hetero atoms; highly eater soluble compounds	Pyridine, phenol, cresols, quinoline, isoquinoline, dibenzophenol,
3	Light aromatic	Usually light hydrocarbons with single ring; Do not pose a problem regarding condensability and solubility	Toluene, ethylbenzene, xylenes, styrene
4	Light poly-aromatic	Two and three ring compounds, condense at low temperature even at very low concentration	Indene, naphthalene, methylaphtalene, biphenyl, acenaphthalene, fluorene, phenanthrene, anthracene
5	Heavy poly-aromatic	Larger than three-rings, these components condense at high temperatures at low concentrations	Fluoranthene, pyrene, chrysene, perylene, coronene

1.8 Biomass tar removal methods

Available methods can be categorized in two types depending on the location where tar is removed, either in the gasifier itself (known as primary method) or outside the gasifier (known as secondary method) [16].

Primary methods (Fig.3) can be defined as all the measures taken in the gasification step itself to prevent or convert tar formed in the gasifier [16]. Secondary methods (Fig. 4) are conventionally used as treatments of the hot gas from the gasifier. These methods can be chemical or physical treatment as follows: (i) tar cracking downstream the gasifier either thermally or catalytically; (ii) mechanical methods such as use of cyclone, baffle filter, ceramic filter, fabric filter, rotating particle separator, electrostatic filter and scrubber, [16].

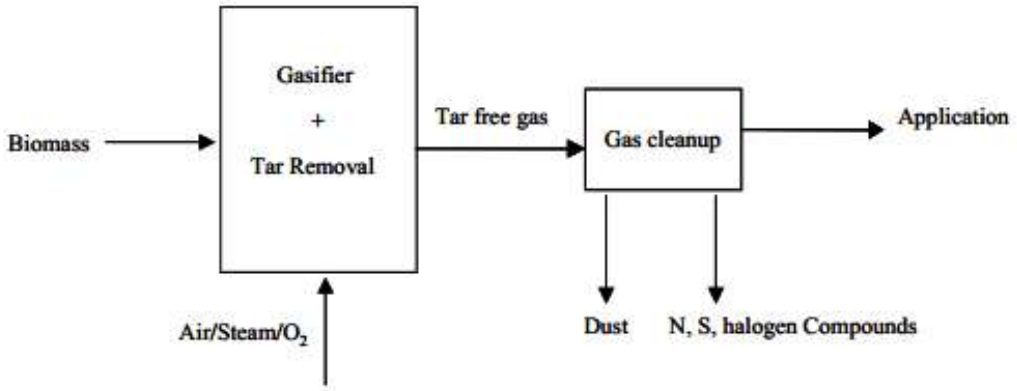

Fig. 3: Tar reduction concept by primary methods [16].

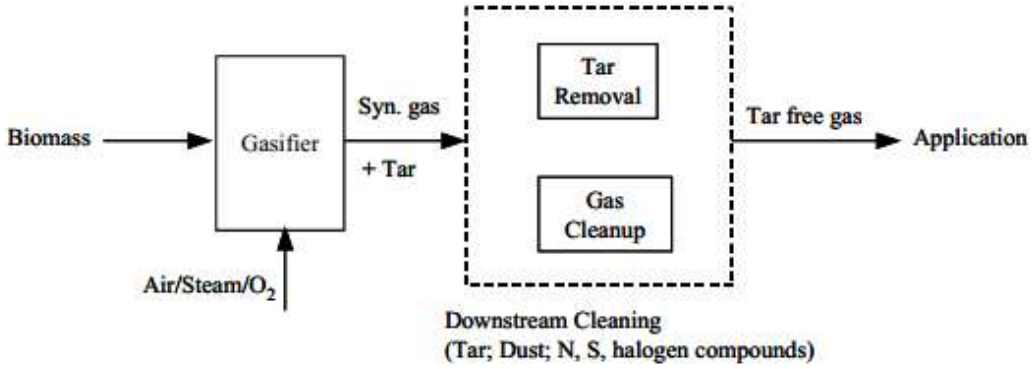

Fig. 4: Tar reduction concept by secondary methods [16].

1.9 Tar removal catalysts

Tar elimination reactions are known to be kinetically limited. Therefore, the reaction rates can be increased by increasing the temperature and/or using a catalyst. However, catalysts can only increase the rate of a reaction that is thermodynamically feasible. Several reactions can occur in a secondary catalytic reactor downstream of the gasifier [14], [17].

The chemistry involved in catalytic tar decomposition of producer gas is a complex mix of hydrocarbon decomposition and equilibrium reactions [14].

The recently develop gas cleaning technique is a catalytic filter. This method combines the filtration for particles removal and catalytic cracking of tar from producer gas in one step. A great amount of experimental results demonstrated that the method is also considerably efficient in removing tar and particles. The schematic diagram of a catalytic filter is shown in Fig.5.

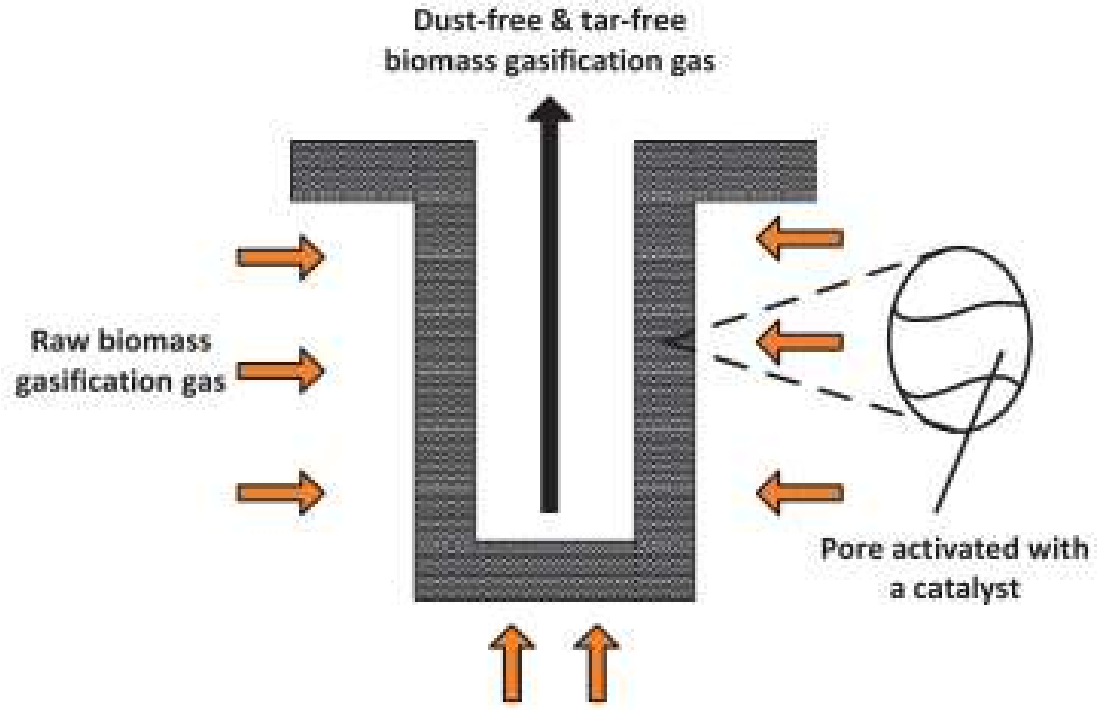

Fig. 5: Schematic representation of a catalytic candle filter [14].

Table 4 summarizes the advantages and disadvantages of different catalysts used for tar removal. A large number of investigations deal with biomass gasification in fluidized bed reactors utilizing nickel catalysts, dolomite or olivine. Supported nickel-based catalysts with various supports and promoters have been the most widely studied class of material, for their high activity and selectivity. However, these catalyst are relative expensive, and their preparation may also be time and energy consuming, thus hindering extensive application of nickel-based catalyst [13]. Besides, these catalysts are susceptible to deactivation from contaminants [14].

The alkali metals, alkaline earth metal oxides (e.g. MgO, CaO), natural ores (e.g. dolomite, olivine) and some clay minerals are also included as basic catalysts. Several studies have been done using these catalysts with considerable reduction tar in their producer gas. Increasing the Ca/Mg ratio, decreasing the grain size, and increasing the active metal content such as iron can improve the activity of these catalysts. The Ca improved the formation of crystal structure and Mg enhanced the degree of carbon structure ordering which played a negative role in gasification. On the other hand, CaO cannot be used as a catalyst at high temperature, because its particles are inclined to agglomerate, resulting in deactivation [18].

The catalytic activity of calcined dolomite was extensively investigated in terms of tar reduction. Calcined dolomite catalyst is more active than the un-calcined dolomite for tar decomposition since its large (internal) surface area and oxide contents on the surface. Calcined dolomite was compared with un-calcined dolomite as well as a calcined olivine and raw olivine as downstream catalysts in steam gasification of apricot stone, and it was found that calcined dolomite is the most effective catalyst for increasing the H_2 content in the gas [18].

Table 4: Advantages and disadvantages of various catalysts for tar removal during biomass gasification [13].

Catalyst	Advantage	Disadvantage
Calcined rocks	Inexpensive and abundant; Attain high tar conversion ~95% conversion with dolomite; Often used as guard beds for expensive catalysts most popular for tar elimination	Fragile material and quickly eroded from fluidized beds
Olivine	Inexpensive; High attrition resistance	Lower catalytic activity than dolomite
Clay minerals	Inexpensive and abundant; Fewer disposal problems	Lower catalytic activity than dolomite; Most natural clays do not support the high temperatures (800-850) needed for tar elimination (lose pore structure)
Iron ores	Inexpensive and abundant	Rapidly deactivated in the absence of hydrogen; Lower catalytic activity than dolomite
Char	Inexpensive and abundant; Sustainable (natural production inside the gasifier); High tar conversion compared to dolomite; Neutral or weak base properties	Consumption because of gasification reaction; Its properties are not fixed depending on biomass type and process conditions
Fluid cracking catalysts (FCC)	Relatively inexpensive but not cheaper than the above; More known about it from experience with FCC units	Rapid deactivation by coke; Lower catalytic activity than dolomite
Alkali-metal-based	Natural production in the gasifier; Reduce ash-handling problems high tar conversion comparable to that dolomite	Particle agglomeration at high temperatures; Lower catalytic activity than dolomite; rapid deactivation by coke

Activated alumina transition-metal-based	Able to attain complete tar elimination at ~900ºC; Increase the yield of CO_2 and H_2; Higher tar reforming activity (NI-based catalyst are 8-10 times more active than dolomite)	Rapid deactivation because of sulfur and high tar content in the feed; Relatively expensive; Relatively easier regenerated

1.10 Olivine-based catalysts

Olivine is the most abundant mineral in the upper mantle of the Earth, occurring predominantly in igneous rocks. It is an orthosilicate with a general formula of $(Fe_xMg_{1-x})_2SiO_4$ representing a complete solid solution between forsterite (Mg_2SiO_4) and fayalite (Fe_2SiO_4). This mineral is rich in Mg and is used as refractory materials in the ceramic and metallurgical industries. Natural olivine has also been recognized as one of the most promising solid materials for use in fluidized bed biomass steam gasification [19].

The catalytic activity of olivine for tar elimination can be related to the magnesite (MgO) and iron oxide (FeO_x) contents. This catalyst is mainly deactivated by the formation of coke, which covers the active sites and reduces the surface area of catalyst. The advantages of this catalyst are its low price and high attrition resistance, mainly when compared to dolomite. The mechanical strength of the catalyst is comparable to sand, even at high temperatures, and its performance is therefore better than dolomite in fluidized-bed environments [14].

Calcination of olivine with air at 900ºC for different treatment times of 1/5/10 h, could improve its activity significantly towards tar removal. Calcination time of 10 h is observed to be the optimal for tar conversion among the tested calcination times [20].

Table 5 shows olivines from different regions and their catalytic activity for naphthalene conversion at representative temperatures.

Table 5: Naphthalene conversion for olivine catalysts as a function of temperature [21]

Region / temperature [ºC]	750	800	850	900
Washington	30	60	80	97
North Carolina	40	75	85	98
Austria	50	90	95	100
Austria-calcined	50	32	62	92

1.11 Objectives of the work

Although natural Fe_2SiO_4 and related natural olivines $(Fe,Mg)_2SiO_4$ are known for their catalytic activity in biomass gasification, corresponding mechanisms are poorly understood, possibly because the exact

composition and other characteristics of natural minerals are ill-defined. Thus, synthetic Fe_2SiO_4 are expected to provide best conditions for detailed catalytic studies. In addition, one may seek alternative multiphase catalysts with additional functionalities such as ability for magnetic separation from ashes, biochars or self-heating ability to sustain the required gasification temperatures and to assist endothermic reactions (e.g. tar reforming); this may be based on composite catalysts containing a second phase with designed electric or magnetic properties for self-heating by ohmic losses or induction (e.g. Fe_2SiO_4-Fe or Fe_2SiO_4-Fe_3O_4) or with suitable dielectric properties for microwave self-heating (e.g. Fe_2SiO_4-SiC).

The present work is focused on the development of a synthetic fayalite (Fe_2SiO_4), the iron rich end member of the olivine solid solution series, with intention of subsequent catalytic studies for the conversion of tars from biomass gasification, in a pilot scale reactor.

The main objectives of this work include:

- to design a procedure for preparation of synthetic fayalite based on silicon carbide as initial reagent, and to study relevant factors affecting the formation of target phase;
- to perform preliminary assessment of catalytic activity of prepared catalyst in a lab-scale reactor;
- to evaluate the possibility of preparation of SiC-Fe_2SiO_4 core-shell catalysts by controlled reactivity between a suitable Fe-precursor and relatively coarse SiC particles (with Fe:Si<2).

The latter objective intents to support hypothesis of having a silicon carbide core with the ability to absorb microwaves, or to deposit a catalytic Fe_2SiO_4 layer on SiC supporting meshes.

II. Experimental

2.1 General synthesis procedure

In order to design a procedure for reproducible preparation of synthetic fayalite, fine silicon carbide powder (Fig. 6, left) was used as a source of silicon. Three iron-containing reagents were tried including hematite, iron nitrate and oxalate (Table 6). On the final stage of the work, coarse-grained SiC powder (Fig. 6, right) was also used to test the possibility of preparation of core-shell structures.

Table 6: Reagents used, name of reagent, provider and purity.

Composition	Name	Provider	purity
Fe_2O_3	Hematite	abcr GmbG	99.8%
$Fe(NO_3)_3*9H_2O$	Iron(III) nitrate nonahydrate	Sigma-Aldrich	99.9%
$FeC_2O_4*2H_2O$	Iron(II) oxalate dihydrate	Sigma-Aldrich	99%
SiC (fine)	Silicon carbide	abcr GmbG	98%
SiC (coarse grained)	Silicon carbide	abcr GmbG	98%

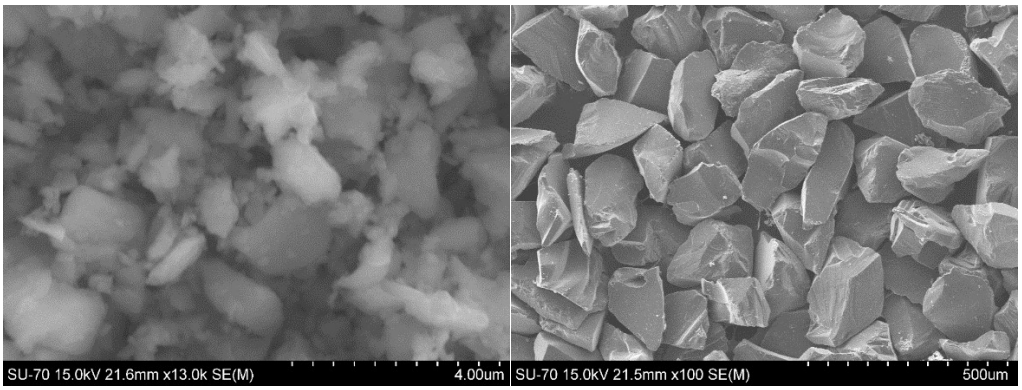

Fig. 6: *SEM micrographs of fine (left) and coarse-grained (right) silicon carbide powders.*

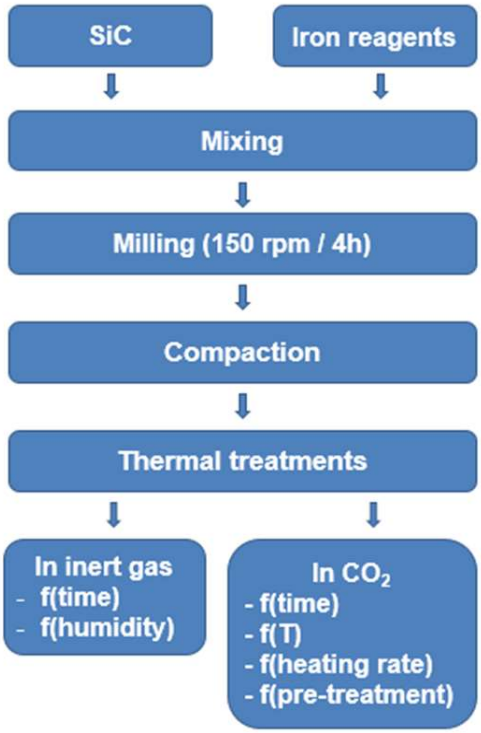

Fig. 7: Scheme of synthesis experiments

The overall scheme of experiments on synthesis of Fe_2SiO_4 is shown in Fig.7. Initial reagents were mixed in agate mortar, and then subjected to ball-milling for better homogenization. Ball-milling was performed using zirconia balls (Tosoh) and nylon container (Fig.8) with ethanol in a Retsch S1 mill at 150 rpm for 4 h.

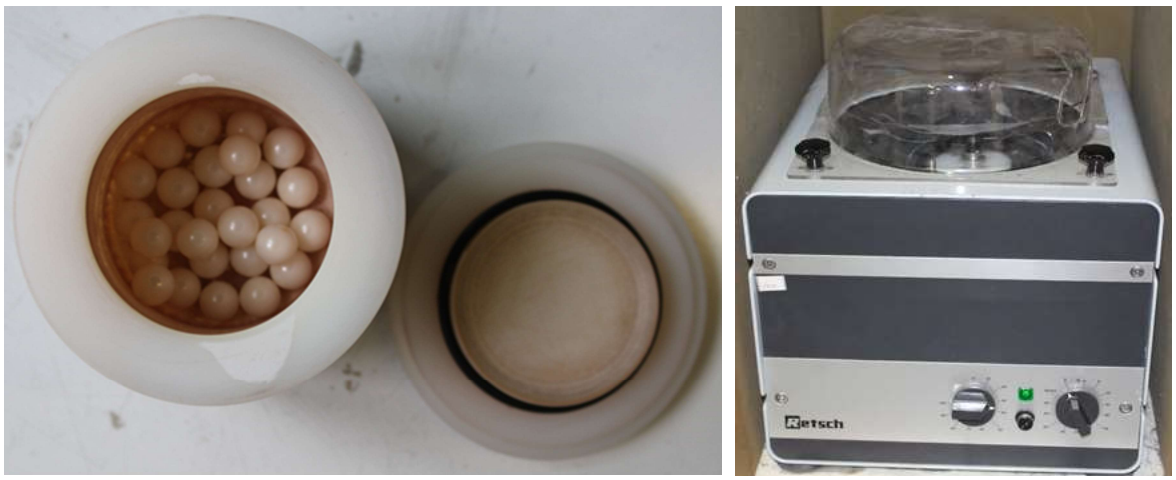

Fig. 8: Nylon container with zirconia balls (left) and Retzsh S1 mill (right)

After milling and drying, the powders were compacted uniaxially into disk-shaped samples (∅ = 10-18 mm) at F = 10 kN using P/O/Weber press (Fig.9). The weight of samples varied between 0.3 and 3 g.

Fig. 9: P/O/Weber manual press.

Compacted samples were subjected to thermal treatment in tubular horizontal furnace with controlled atmosphere (Fig.10). The treatment program was varied in order to evaluate the impact of different factors on reactivity and phase formation. The relevant parameters included:

- initial Fe-containing reagent;
- atmosphere;
- humidity (dry of humidified gas flow);
- temperature of isothermal treatment;
- time of isothermal treatment;
- heating/cooling rate.

Humidification of flowing gas was done by bubbling the gas through water in a Drechsel bottle at the inlet of the furnace. The thermal treatment profile was modified in the course of experiments based on the results.

Another relevant factor was pretreatment of reagent mixture by high-energy milling before compaction. High-energy milling was performed using zirconia ball and vial using Retsch PM 100 planetary ball mill, with the planetary rotation of 600 rpm and the vial rotating at 1200 rpm in the opposite direction, for 4 h.

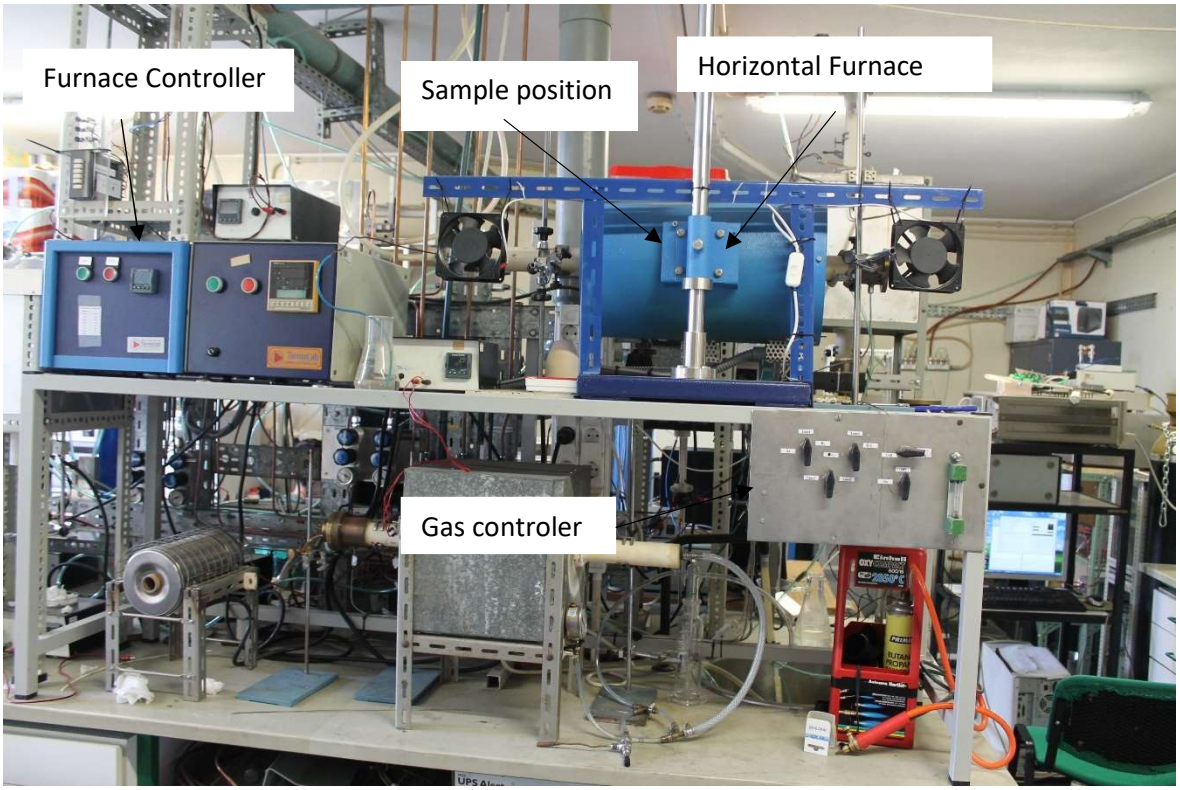

Fig. 10: Tubular furnace used for thermal treatments.

2.2 X-ray diffraction

X-ray diffraction (XRD) is one of the most important and most powerful methods for the investigation of the material. These methods are based on the scattering of X-rays by the electrons of atoms. The wavelengths of X-rays are similar to interatomic distances, and so the X-rays scattered by different atoms will interfere destructively or constructively, in the latter case giving rise to diffracted beams [22].

The geometry of the corresponding diffraction events can be described by Bragg's law, which combines the distance (d) between lattice planes the wavelength λ of the X-ray radiation and the diffraction angle (θ), [22]:

$$2d\sin(\theta)=\lambda \qquad \text{Eq. 1}$$

The Bragg equation treats diffraction as the reflection of X-rays at the lattice planes [22].

By analyzing the geometry of the diffracted beams, the information can be gained on the geometry of the lattice of the structure under investigation. By further analyzing the intensity distribution of the reflection, information on the positions of the atoms can be obtained. This is usually carried out by measuring X-ray reflections on a single-crystal and forms the basis of X-ray single-crystal structural analysis [22].

XRD patterns of powdered samples were collected using PANalytical X'Pert Alpha-1 (CuKα1 radiation, 2θ range = 10-80°).

2.3 Scanning electron microscopy

Scanning electron microscopy (SEM) primarily for the study of surface topography and morphology of solid materials on a scale down to about 10 nm, topographical features, void content, particles agglomeration as well as compositional and structural differences within the material can be revealed [22].

The technique works on the principle that an electron beam is passing through an evacuated column and focused by electromagnetic lenses onto the material. The beam is scanned over the specimen surface in synchronism with the beam of cathode ray tube (CRT) display screen [22].

SEM micrographs were obtained using Hitachi SU-70 microscope.

2.4 Thermogravimetric analysis

Thermogravimetric analysis (TGA) is a technique in which an alteration in the mass of the sample is analysed while the sample is subjected to a change of temperature [23]; this may be performed in controlled atmospheres. TGA was performed using Setaram SetSys 16/18 analyser (sensitivity 0.4 μg, initial sample weight ~100 mg) in a flow of CO_2 at 5°C/min.

2.5 Gasification reactor

The experimental facility included a thermally insulated pilot-scale 75 kWth bubbling fluidized bed reactor (BFB) made of AISI 310 SS with a reaction chamber of 0.25 m internal diameter and 2.3 m height, developed at the University of Aveiro (Fig. 12). The bottom bed of the reactor has a (static) height of 0.23 m and is composed by sand (high quartz content, particles with size in range 355 μm – 1000 μm); 17 kg of sand composed the bottom bed. Dry atmospheric air used as gasification agent, fed through the distributor plate. The biomass is fed at the bed surface, 0.30 m above the distributor plate, by means of a screw feeder [24].

The star-up of the reactor until an operating bed temperature of around 500 ºC was performed by a propane burner and by pre-heating the primary air. After reaching a bed temperature of around 500 ºC, the biomass feeding was started and the gas burner and primary air pre-heating system were switched off. Afterwards, the biomass combustion allowed the delivery of the necessary heat to achieve the desired operating bed temperatures and the equivalence ratio was controlled at the wanted level by adjusting the biomass feeding rate while keeping the primary air gas flow rate constant. Then, the direct gasifier was operated under autothermal and steady-state conditions without any external auxiliary heating systems, with the necessary heat for the gasification systems, thus with the necessary heat for the gasification process delivered from the partial combustion of the biomass fuel in the reactor [24].

The fluidized bed was operating at atmospheric pressure and in bubbling regime, with superficial gas velocity of around 0.28-0.30 m/s (depending on the operating conditions, namely the bed temperature), and with average bed temperatures in the range of 700 ºC to 870 ºC. The bed temperature was maintained at the desired level by regulating the insertion of a set of eight water-cooled probes located at the bed level [24].

The fuel used (table 7) in the gasification experiments included commercial pine pellets (6mm diameter and 15mm – 20 mm length), [24]. For a detailed analysis of syngas, a SRI 8610C Gas Chromatograph was used.

Table 7: Fuel used in the gasification reactor.

Fuel	Supplier	Quality
Propane gas	OZ energia	
Biomass pellets	Pinewells	EN plus A1

The pilot-scale gasification installation consists of several systems (Fig. 11 layout of gasification system and Table 8 legend of Fig. 11):

- Reactive
  - Biomass feed;
  - Air supply;
  - Refrigeration;
- Monitoring of operation;
- Sampling and gas analysis;
- Data acquisition;
- Combustion of gasification gases.

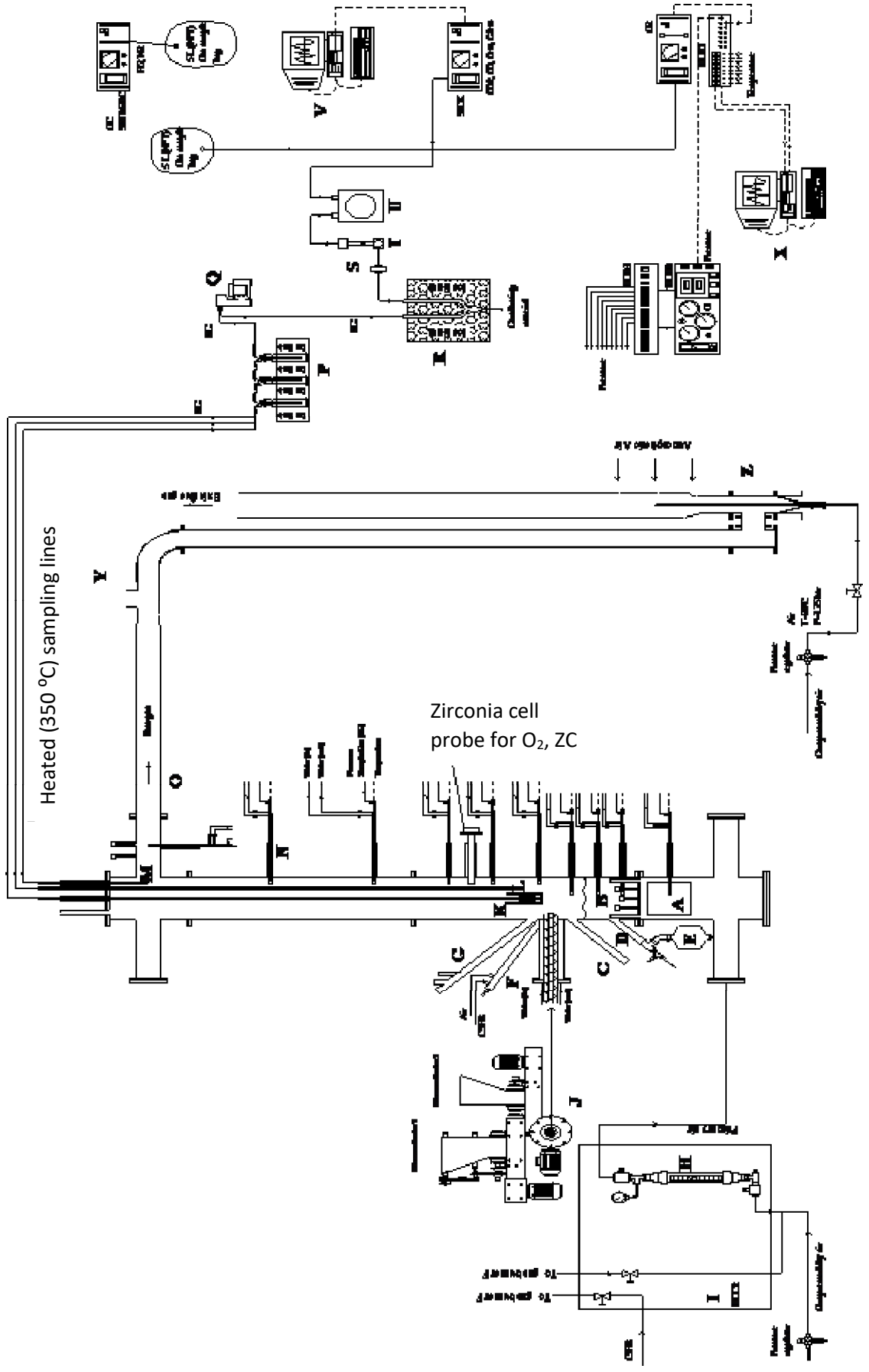

Fig.11: Schematic layout of the experimental gasification facility with a pilot-scale BFB reactor. Legend in Table 8.

Table 8: Legend of Fig.11.

Position	Name
A	Primary air heating system
B	Sand bed
C	Bed solids level control
D	Bed solids discharge
E	Bed solids discharge silo
F	Propane burner for preheating
G	Port for visual inspection of bed surface
H	Air flow meter (primary air)
I	Control and command unit UCC2
J	Biomass feeder
K	Reactor with catalyst
L	Reactor without catalyst
M	Raw gas sampling probe
N	Water-cooled probe for gas sampling pressure and temperature monitoring
O	Gas exhaust
P	Gas condensation unit with impingers for condensable gases (water, tars) removal
Q	Gas sampling pump
R	Gas condensation unit for moisture and other condensable gases removal
S	Filter for particle matter/aerosol removal
T	Gas flow meter
U	Dry gas meter
V	Computer for data acquisition from SICK analyser
X	Computer for data acquisition and control system
Y	Security exhaust pipe
Z	Raw gas burner

The reactive system consists of a pilot scale BFB reactor and a set of accessory organs that allow reactor operation. The set of accessory organs includes: Control Unit and Control Unit 2 (UCC2) (I, Fig. 11), which supports the electric control circuit of the reactor operation and the pneumatic gas circuit, the auxiliary unit for cooling water and the biomass feed unit (J, Fig.11).

The monitoring system consists of several probes arranged along the reactor (N, Fig. 11), which allow the measurement of temperature and pressure through nine thermocouples and a pressure sensor, respectively, and a zirconium probe for measurement of oxygen (ZC, Fig. 11)

The gas sampling and analysis system consist of two lines, thermally insulated and heated 350 ºC, three probes for gas sampling at the exhaust (M, Fig. 11), and gas above the bed surface (K and L, Fig. 11) a pump (Q, Fig. 11), a filter for particulate material (S, Fig. 11), a dry gas meter (U, Fig. 11), two condensation systems for water and tar removal (R and P, Fig. 11), a rotor (T, Fig. 11) and three gas composition analysers, namely:

- Non-dispersive online infrared analyser CO, CO_2, CH_4 and C_2H_4 (GMS-810 SICK);
- Paramagnetic O_2 analyser (model ADC-700 with Servomex module);
- Thermal conductive detector (TCD, SRI 8610C Gas Chromatograph).

The data acquisition is carried out by two computers, one that allows the reception of the information obtained by the SICK analyser through the SOPAS software and temperature registered in the three Testo 176

T4 through the software ComSoft Basic 5 SP5 (V, Fig. 11) and one for temperature and pressure data obtained through the electronic multiplexing circuit installed in the UCE (X, Fig. 11). The latter works with your own software developed in Quick-Basic.

The gasification combustion system (Z, Fig. 11) consist of a burner which aims to eliminate the pollutants present in the gas produced, which are dangerous to human health and the environment, such as CO, CH_4 and tar. The burner eliminates the pollutants by burning the gas so that it contains mostly CO_2 and H_2O and can be released into the atmosphere in a safer way. The aim of this system is the possibility of conducting biomass gasification experiments without affecting the quality of the air outside the installation

Fig.13 indicated the position of the catalyst sample in the reactor, and the Fig.14 shows the catalyst container, scheme of catalyst placement in the container, and inner part of reactor.

Fig.12: Gasification reactor.

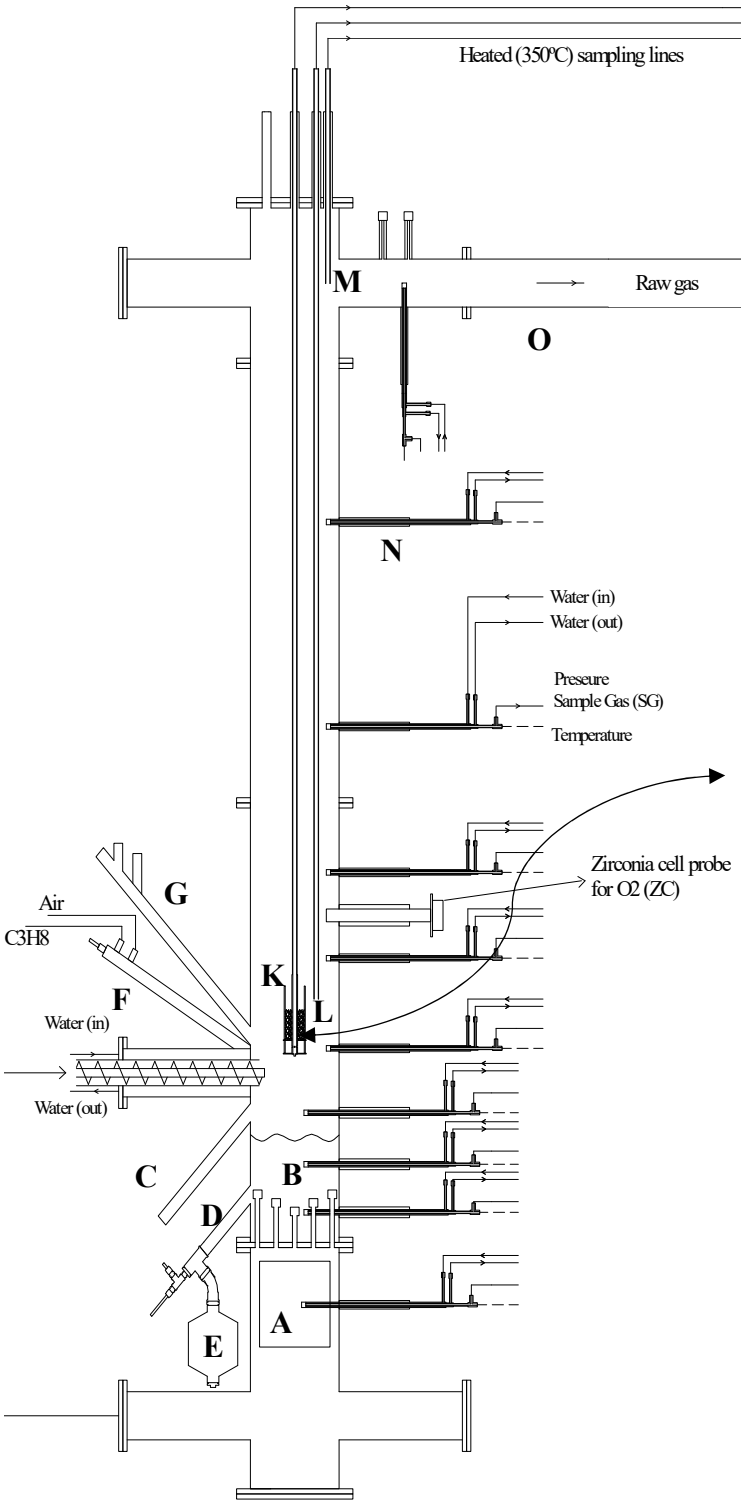

Fig. 13: Location of the catalyst sample in the reactor. (detail of Fig. 11).

Fig.14: Catalyst container and the position where catalyst is placed in the container (left); inner part of the reactor (right).

III. Results and discussion

3.1 Thermodynamic guidelines for Fe_2SiO_4-based catalysts

3.1.1 Fundamentals of activity diagrams

The thermodynamic analysis was based on activity diagrams as proposed by Yokokawa [25] and applied to a variety of systems, including the complex chemistry of cementitious materials [26]. The method is based on derivation of representative reactions for 2-phase equilibria, as shown in Table 9, and then extracting the relevant values of pO_2, $a_{Fe} : a_{Si}$ activity ratio, or $a_{Fe} : a_{Si}$ vs pO_2, from the relevant mass action constant. These relations are made explicit by distinguishing the following types of 2-phase equilibria, with suitable stoichiometric coefficients:

- 2-phase equilibria which depend only on redox conditions (e.g. $O_2 \rightarrow 2FeO$ for Fe/FeO equilibrium). These reactions are expressed per mole of O_2, to yield a direct relation between pO_2 and mass action constant;
- 2-phase equilibria which depend on ($a_{Fe} : a_{Si}$) activity ratio (e.g. $Fe_2SiO_4 + Fe \rightarrow Fe_3O_4 + Si$ for Fe_2SiO_4/Fe_3O_4). These reactions are expressed per mole of Fe on reactant side (combined with the Fe-lean phase) and per mole of Si on product side, combined with the Si-lean phase, as exemplified by $SiO_2 + Fe \rightarrow 0.5Fe_2O_3 + Si + 0.25O_2$ for SiO_2/Fe_2O_3. The remaining stoichiometric coefficients are then readily obtained by solving the elemental balances for Fe, Si and O; this includes the stoichiometric coefficient of molecular O_2 if this is required to compensate for oxygen imbalance of the solid phases.

The resulting 2-phase equilibria are listed in Table 9, and relevant relations (Eq. 2 to Eq. 6) were used to compute the corresponding Gibbs free energy of reaction, and mass action constants $k = \exp(-\frac{\Delta G_R}{RT})$. Required thermodynamic properties are the standard formation enthalpies (ΔH_i^o), standard entropies (ΔS_i^o) and heat capacities (Cp_i), which were retrieved from a commercial database and software package FACTSAGE v5.5 [27], with additional information from reference Jacobs [28].

$$\Delta G_R = \Delta H_R - T\Delta S_R \quad \text{Eq. 2}$$

$$\Delta H_R^o = \sum a_i \, \Delta H_{f\,prod}^o - \sum a_j \, \Delta H_{f\,reag}^o \quad \text{Eq. 3}$$

$$\Delta S_R^o = \sum a_i \, S_{i\,prod}^o - \sum a_j \, S_{j\,reag}^o \quad \text{Eq. 4}$$

$$\Delta H_R = \Delta H_R^o + \sum a_i \int_{298K}^{T} c_{p_{prod}} dT - \sum a_j \int_{298K}^{T} C_{p_{reag}} dT \quad \text{Eq. 5}$$

$$\Delta S_R = \Delta S_R^o + \sum a_i \int_{298}^{T} \left(\frac{C_p}{T}\right)_{prod} dT - \sum a_j \int_{298}^{T} \left(\frac{C_p}{T}\right)_{reag} dT \quad \text{Eq. 6}$$

Table 9: Thermodynamic prediction for interaction of solid phases in the system Fe-Si-O

Boundary	Reaction	Relation
$Fe/SiO_2/C$	$Si + O_2 \rightarrow SiO_2$	$\log\left(\frac{a_{Fe}}{a_{Si}}\right) = \frac{\Delta G_R}{2.30RT} + \log(pO_2)$
$C/SiC/SiO_2$	$SiC + O_2 \rightarrow SiO_2 + C$	$\log(pO_2) = \frac{\Delta G_R}{2.30RT}$
SiO_2/Fe_3O_4	$Fe + SiO_2 \rightarrow \frac{1}{3}Fe_3O_4 + Si + \frac{1}{3}O_2$	$\log\left(\frac{a_{Fe}}{a_{Si}}\right) = \frac{\Delta G_R}{2.30RT} + \frac{1}{3}\log(pO_2)$
FeO/Fe	$2Fe + O_2 \rightarrow 2FeO$	$\log(pO_2) = \frac{\Delta G_R}{2.30RT}$
Fe_3O_4/FeO	$6FeO + O_2 \rightarrow 2Fe_3O_4$	$\log(pO_2) = \frac{\Delta G_R}{2.30RT}$
Fe_2O_3/Fe_3O_4	$4Fe_3O_4 + O_2 \rightarrow 6Fe_2O_3$	$\log(pO_2) = \frac{\Delta G_R}{2.30RT}$
Fe/Fe_3O_4	$\frac{3}{2}Fe + O_2 \rightarrow \frac{1}{2}Fe_3O_4$	$\log(pO_2) = \frac{\Delta G_R}{2.30RT}$
SiO_2/Fe_2O_3	$SiO_2 + Fe \rightarrow \frac{1}{2}Fe_2O_3 + Si + \frac{1}{4}O_2$	$\log\left(\frac{a_{Fe}}{a_{Si}}\right) = \frac{\Delta G_R}{2.30RT} + \frac{1}{4}\log(pO_2)$
SiO_2/Fe_2SiO_4	$\frac{3}{2}SiO_2 + Fe \rightarrow \frac{1}{2}Fe_2SiO_4 + Si + \frac{1}{2}O_2$	$\log\left(\frac{a_{Fe}}{a_{Si}}\right) = \frac{\Delta G_R}{2.30RT} + \frac{1}{2}\log(pO_2)$
Fe_3O_4/Fe_2SiO_4	$Fe_2SiO_4 + Fe \rightarrow Fe_3O_4 + Si$	$\log\left(\frac{a_{Fe}}{a_{Si}}\right) = \frac{\Delta G_R}{2.30RT}$
$Fe/SiC/C$	$SiC \rightarrow Si + C$	$\log\left(\frac{a_{Fe}}{a_{Si}}\right) = \frac{\Delta G_R}{2.30RT}$

3.1.2 Thermodynamic guidelines for the synthesis of Fe_2SiO_4

The thermodynamics of the Fe-Si-O-C system was examined to provide a guideline for redox conditions required to adjust selective secondary phases (Fig.15). These room temperature thermodynamic predictions show that Fe_2SiO_4 may coexist with metallic Fe or magnetite and indicate the corresponding redox ranges.

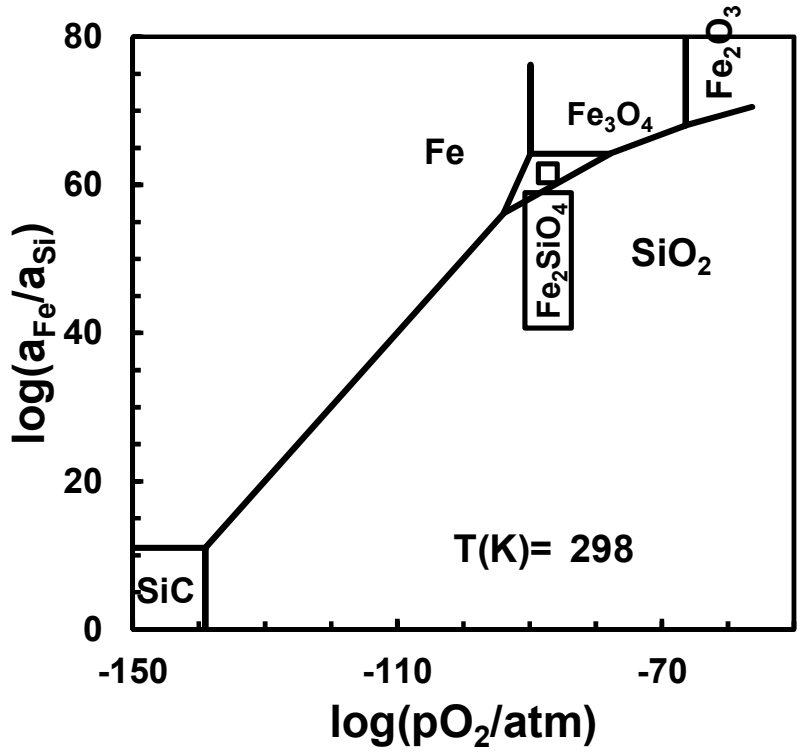

Fig. 15: Thermodynamic prediction for the Fe-Si-O system at room temperature, to assess prospects for direct mechanochemical synthesis from SiC+Fe_2O_3 or other precursors mixtures.

However, the chemical potential differences between the ternary point Fe+Fe_3O_4-Fe_2SiO_4 and the binary Fe_2SiO_4/SiO_2 interface are relatively low to ensure fast reactivity, at least for direct mechanosynthesis at room temperature. Note that the small range of activity ratio (a_{Fe}/a_{Si}) across the stability range of Fe_2SiO_4 corresponds to relatively small chemical potential differences, as given by:

$$\Delta \log\left(\frac{a_{Fe}}{a_{Si}}\right) = \frac{\Delta\mu_{Fe} - \Delta\mu_{Si}}{2.303RT} \qquad \text{Eq. 7}$$

One the contrary, wide chemical potential gaps between SiC and Fe_2O_3 suggest much higher reactivity. Nevertheless, the oxygen contents is not enough to ensure complete oxidation of SiC. Thus, formation of Fe_2SiO_4 requires additional oxygen supply as follows:

$$SiC + Fe_2O_3 + 1.5O_2 \rightarrow Fe_2SiO_4 + CO_2 \qquad \text{Eq. 8}$$

Otherwise, one may use highly oxidizing Fe precursors (e.g. nitrate) to attempt mechanochemical synthesis as follows:

$$SiC + 0.8Fe_2O_3 + 0.4Fe(NO_3)_3.nH_2O \rightarrow Fe_2SiO_4 + CO_2 + 0.6N_2 + 0.4nH_2O \qquad \text{Eq. 9}$$

Actually, this failed, probably due to the high hygroscopic behaviour of Fe-nitrate.

Another method may be based on firing SiC+ Fe_2O_3 powder mixtures in contact with wet atmospheres [29] or atmospheres containing CO_2 [30]; this promotes active oxidation of SiC to SiO_2 in contact with the corresponding H_2/H_2O or CO/CO_2 redox pairs, even in ceramic samples or films , mainly at temperatures above 1200ºC. Wet atmospheres often provide conditions for faster reactivity, even when compared to pure O_2,

mainly by inducing porosity and preventing passivation [29]. On the contrary, CO_2 is less reactive but is likely to allow greater flexibility for controlled redox induced reactivity, mainly by adjusting the r=CO:CO_2 ratio, i.e.:

$$SiC+Fe_2O_3+\gamma CO_2 \rightarrow Fe_2SiO_4+\frac{r(1+\gamma)}{1+r}CO+\frac{1+\gamma}{1+r}CO \qquad \text{Eq. 10}$$

Thermodynamic conditions for redox dependence on H_2/H_2O and CO:CO_2 ratios are, thus, shown in Fig.16, to emphasize the close matching between these conditions and redox stability of Fe_2SiO_4, revealed by the expanded scales (Fig.16, right). This suggests conditions for synthesis of Fe_2SiO_4 with those redox pairs. Actually, the ratio between reduced and oxidised species will vary by reactions of SiC with the oxidised species (i.e. $SiC+2CO_2 \rightarrow SiO_2+2CO$ or $SiC+2H_2O \rightarrow SiO_2+H_2$). Thus, easier control of reaction $SiC+2CO_2 \rightarrow SiO_2+2CO$ is best suited to adjust the CO:CO_2 ratio to suitable redox conditions for Fe_2SiO_4. The experimental demonstration can be performed by varying the conditions of heat treatment, such as temperature and time. Controlled kinetics is also needed to prevent carbon deposition, which would be promoted by the combination of excessively reducing conditions and catalytic activity of metallic Fe.

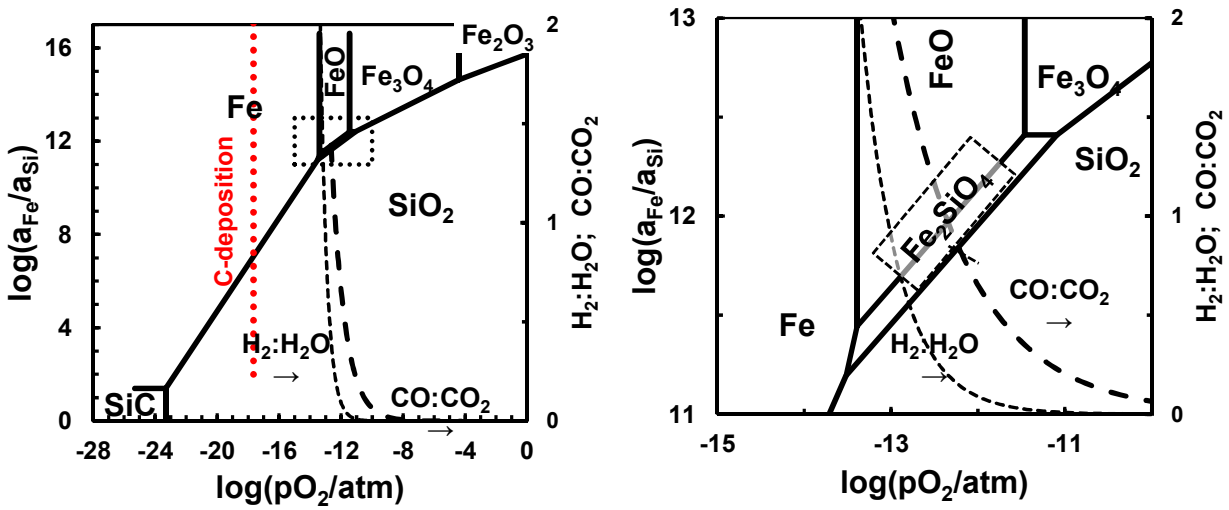

Fig. 16: Thermodynamic calculations at 1373 K for Fe-Si-O-C, and superimposed calculations for H_2-H_2O and CO-CO_2 atmospheres, including the transition from carbon-deposition to carbon-free conditions (vertical dotted line) (top). An extended range (right) is shown to emphasise that the stability range of Fe_2SiO_4 reduces to narrow redox and chemical potential ranges.

3.1.3 Thermodynamics of Fe_2SiO_4 under biomass-gasification

The intrinsic oxygen contents in biomass is usually more suitable for its pyrolysis, i.e., for simultaneous formation of vegetable carbon and partial gasification. Thus, additional supply of oxygen needed to reach the highest contents of carbon monoxide or syngas with adjustable H_2:CO ratio, as revealed by the thermodynamic calculations in Fig.17, at 973K.

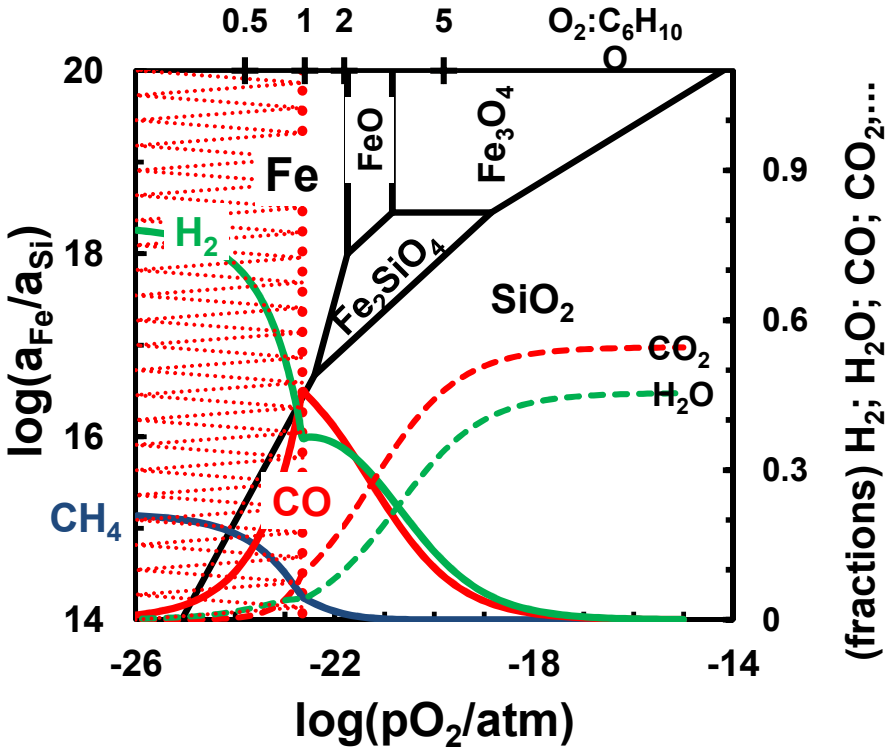

Fig. 17: Thermodynamic predictions of redox stability in the Fe-Si-O system at 973K superimposed on the redox conditions expected for gasification of cellulose, with different O_2:$C_5H_{10}O$ ratios, shown in the secondary horizontal axis. The shaded area shows conditions for co-existence of carbon and partial gasification.

Also, additional oxygen is needed if one seeks nearly autothermal conditions by partial oxidation. In this case, thermodynamic calculations predict that the highest yield of carbon monoxide should be attained for O_2:$C_5H_{10}O$≈1:1, at the transition from carbon-deposition to carbon-free conditions; this is also close to the ternary point Fe/Fe_2SiO_4/SiO_2. Thus, thermodynamic predictions are consistent with empirical demonstration that Fe_2SiO_4 is an active biomass gasification catalyst. On the contrary, the stability of Fe oxides (wustite or magnetite) or their coexistence with Fe_2SiO_4/SiO_2 corresponds to redox conditions with significant fractions of fully oxidised gases (CO_2 and H_2O).

3.2 Synthesis of Fe_2SiO_4

3.2.1 Reaction of Fe_2O_3+SiC powder mixtures under inert gas atmosphere

It was found that treatments of Fe_2O_3+SiC precursors under dry Ar gas flow (Fig.18) imposes unsuitable conditions, probably because the oxygen content in the gas flow is residual (pO_2≈10^{-5} atm) and the actual oxygen content of hematite only accounts for oxidation of SiC, whereas hematite is reduced to metallic Fe. One may assume that the overall carbon balance may comprise contributions of partial oxidation to CO and complete oxidation to CO_2, and possibly even traces of carbon deposition:

$$SiC + \frac{2 + x + 2y}{3} Fe_2O_3 \rightarrow SiO_2 + xCO + yCO_2 + (1 - x - y)C + \frac{4 + 2x + 4y}{3} Fe \quad \text{Eq. 11}$$

Formation of a coherent (and highly redox stable) SiO_2 scale may, then, passivate the SiC phase by preventing direct reaction between SiC and Fe_2O_3. In fact, the phase stability diagram also shows that redox and chemical potential gradients vanish at the ternary Fe-SiO_2-Fe_2SiO_4 point. Thus, onset of Fe and SiO_2 at early stages may suppresses the effective driving force, hindering subsequent transformation to Fe_2SiO_4.

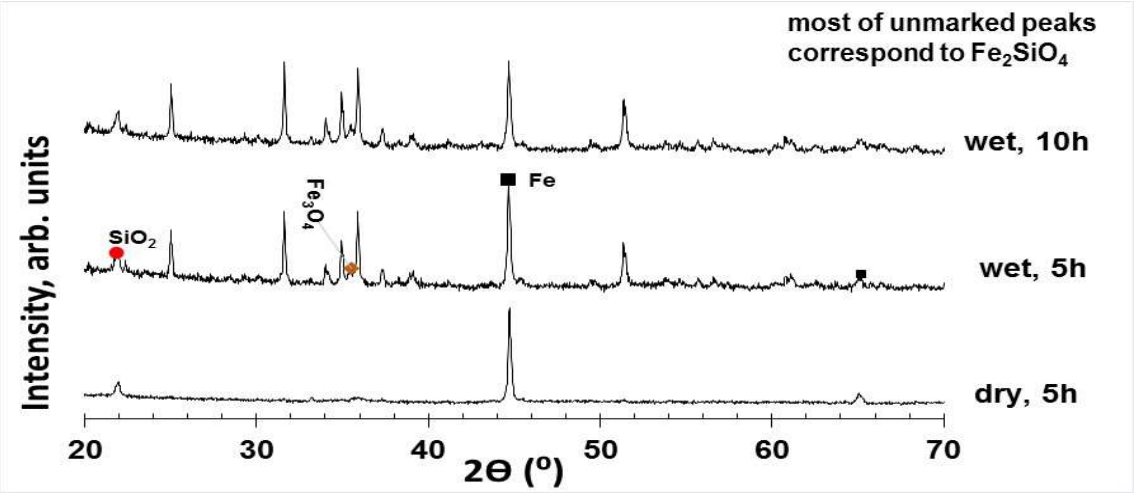

Fig. 18: XRD of pelletized samples (SiC+Fe_2O_3) after treatment in Ar at 1100°C. Initial sample weight ≈0.3 g.

Humidified inert atmosphere (Fig. 18) provides better conditions to promote formation of fayalite, possibly because steam provides the required oxygen supply, and SiC reacts readily in wet atmospheres, [31]without passivation; this may enable the alternative mechanism described by Eq.12. However, fayalite still coexists with SiO_2 and metallic Fe, suggesting that both reactions (Eqs.11 and 12) coexist. In addition, faster reactivity of SiC in wet atmospheres may contribute to earlier extinction of SiC, as indicated by increase of relative intensity of SiO_2 reflections, and readier evolution to less reducing conditions, revealed by onset of Fe_3O_4.

$$SiC + Fe_2O_3 + (1+x+2y)H_2O \rightarrow Fe_2SiO_4 + xCO + yCO_2 + (1-x-y)C + (1+x+2y)H_2 \quad \text{Eq. 12}$$

The use of iron nitrate as initial reagent under identical treatment provides even slightly more oxidizing conditions, as emphasized by the relative intensity of SiO_2 reflection; still, XRD also showed the presence of metallic iron, in addition to crystobalite SiO_2 and traces of other phases in addition to the main fayalite phase (Fig. 19). Presence of metallic Fe may be explained by early decomposition of Fe nitrate to iron oxides on heating, i.e.:

$$2Fe(NO_3)_3 * 9H_2O \rightarrow Fe_2O_3 + 18H_2O + 3N_2 + 7.5O_2 \quad \text{Eq. 13}$$

Thus, this highly oxidant precursor may decompose too early, before onset of its reactivity with SiC. The presence of metallic Fe (Fig.19) shows that the oxygen supply has been depleted before complete reactivity of SiC. In addition, the resulting gases (O_2 and humidity) evolved by early decomposition of the nitrate precursor

are known to promote direct oxidation of SiC to SiO_2, at lower temperatures [25], This explains why a fully oxidized phase co-exists with the reduced metallic phase in the final product.

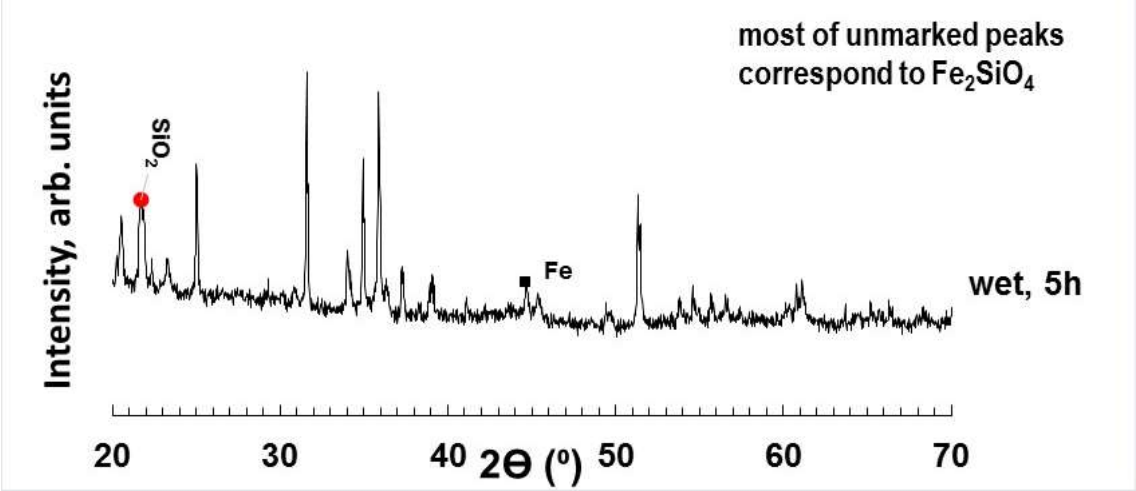

Fig. 19: XRD of pelletized samples (SiC + $Fe(NO_3)_3$*$9H_2O$) after treatment in Ar at 1100°C. Initial sample weight ≈0.3 g.

3.2.2 Initial treatments in CO_2 atmosphere

It was found that CO_2 flow also supplies enough oxygen to prevent onset of metallic Fe, as shown in Fig. 20. However, kinetics of reactions seems insufficient at 1000ºC. Co-existence of magnetite, as major phase, with smaller fractions of fayalite shows that SiC still reacts partially with hematite at 1000ºC, and this may be described by:

$$xSiC+Fe_2O_3 \rightarrow xFe_2SiO_4+\left(\frac{3}{4}\text{-}1.5x\right)Fe_3O_4+xCO_2 \qquad \text{Eq. 14}$$

Note also that silica could not be detected in this case, in spite of its high thermodynamic stability even at much lower temperatures (Fig. 17), suggesting that the $a_{Fe} : a_{Si}$ activity ratio remains relatively high, most probably close to the 2-phase Fe_3O_4/Fe_2SiO_4 equilibrium, and in a relatively narrow redox range. However, this raises questions about the overall Si:Fe ratio, which deviates from the nominal 1:2 ratio in Eq.13, unless one considers also presence of amorphous phase (e.g. silicon oxycarbide SiCO) undetected by XRD. It is readily formed by pyrolysis of sol-gel or silicone resins [32] and though onset of SiCO seems unlikely in common processing conditions, this remains an open question.

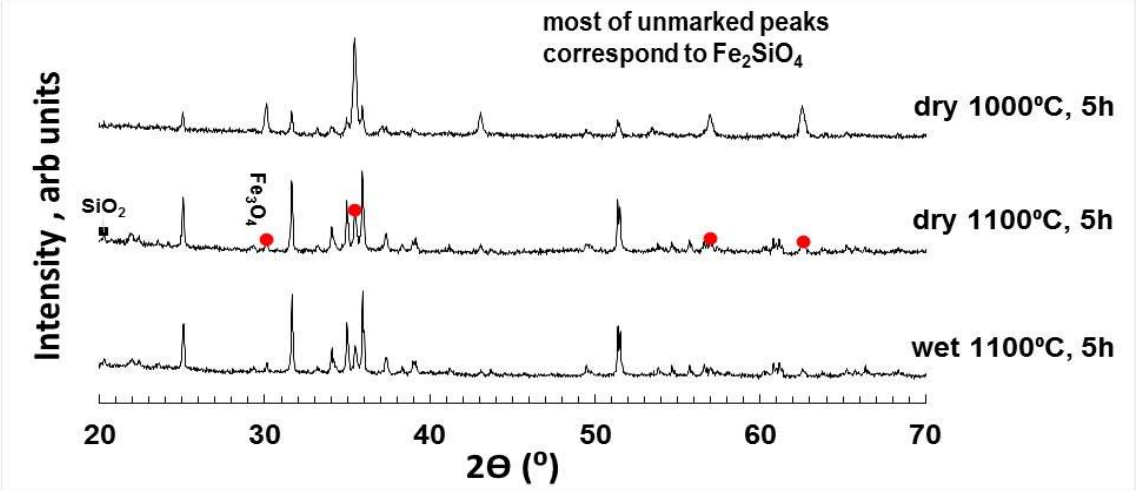

Fig. 20: XRD patterns of pelletized samples ($SiC+Fe_2O_3$) after treatment in dry and wet CO_2 flow at 1000-1100°C. Initial sample weight ≈0.3 g.

Onset of Fe_2SiO_4 as a major phase only occurs readily at about 1100ºC and, in this case, humidification was observed to have rather negligible effect upon treatment in wet CO_2 flow. One observes clearly onset of crystalline silica (Fig. 20) though still with much smaller reflections compared to the fayalite and magnetite phases.

3.2.3 Treatments in CO_2: effect of time

The results indicate that increasing thermal treatment time in a flow of dry CO_2 at 1100 ºC promotes the oxidation of target fayalite phase and leads to a gradual transformation to a mixture of silica and magnetite (Fig 21). The best results are obtained for shortest time at 1100ºC (basically, heating to 1100°C followed by immediate cooling) yielding the nearly pure target Fe_2SiO_4 phase. Thus, one can optimize the supply of CO_2 to promote controlled reactivity of SiC and to avoid onset of metallic Fe, while avoiding undue subsequent oxidation of the fayalite phase.

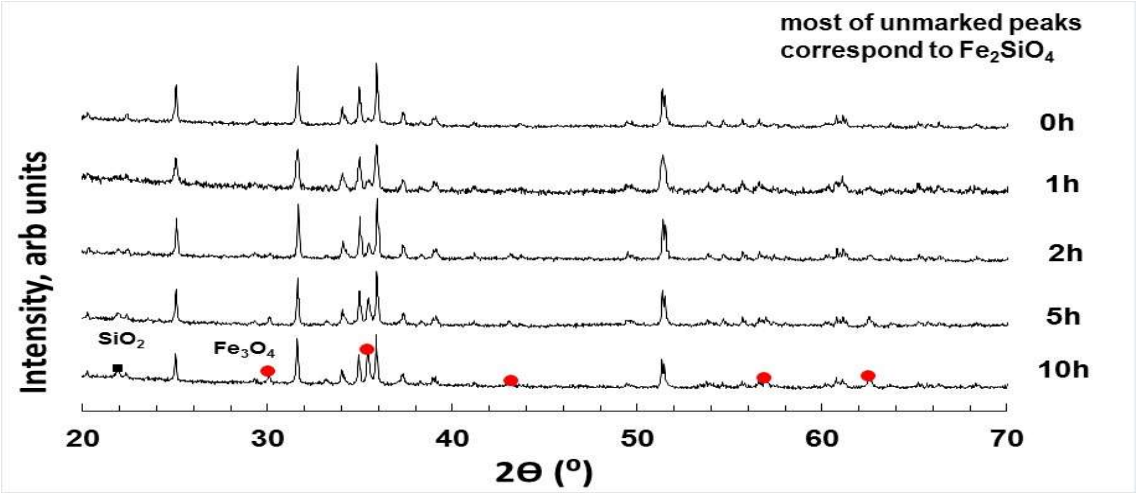

Fig. 21: XRD of pelletized samples ($SiC+Fe_2O_3$) after treatment in dry CO_2 flow for different times at 1100°C. Initial sample weight ≈0.3 g.

3.2.4 Effects of heating rate, mechanical pre-treatment and compaction

In order to further evaluate the relevant factors affecting the reactivity between SiC and Fe_2O_3 under CO_2 atmospheres, three series of samples were subjected to thermal treatment on CO_2. The samples included powdered precursors obtained by normal milling (150 rpm), and compacted precursors either prepared by normal milling or additionally pre-treated in high-energy mill (4 h, 600 rpm). Thermal treatment procedure included heating to 1100°C at different rate with immediate subsequent cooling with the same rate.

It was found that, for each type of samples, decreasing heating/cooling rate basically increased thermal treatment time at elevated temperatures, promoting oxidative formation of magnetite and silica (Fig..22), possibly by transformation of Fe_2SiO_4. However, the effects of heating rate on the reactivity of ball-milled SiC+Fe_2O_3 mixtures (Fig.22) seems surprising, namely because one would expect more extensive oxidation of SiC to SiO_2 under the lowest heating rate, which corresponds to longest time scale. The actual results show the opposite trend, possibly because slower heating allows conditions for passivation of SiC, yielding a coherent sub-micro protective scale. Note that SiC shows much higher oxidation resistance under conditions of favourable passivation, than for non-passivated conditions [31]. In addition, the X-ray diffractograms for lower heating rates show lower Fe_2SiO_4:Fe_3O_4 reflection ratios, also suggesting that earlier passivation hinders subsequent direct reactivity of SiC with Fe_2O_3.

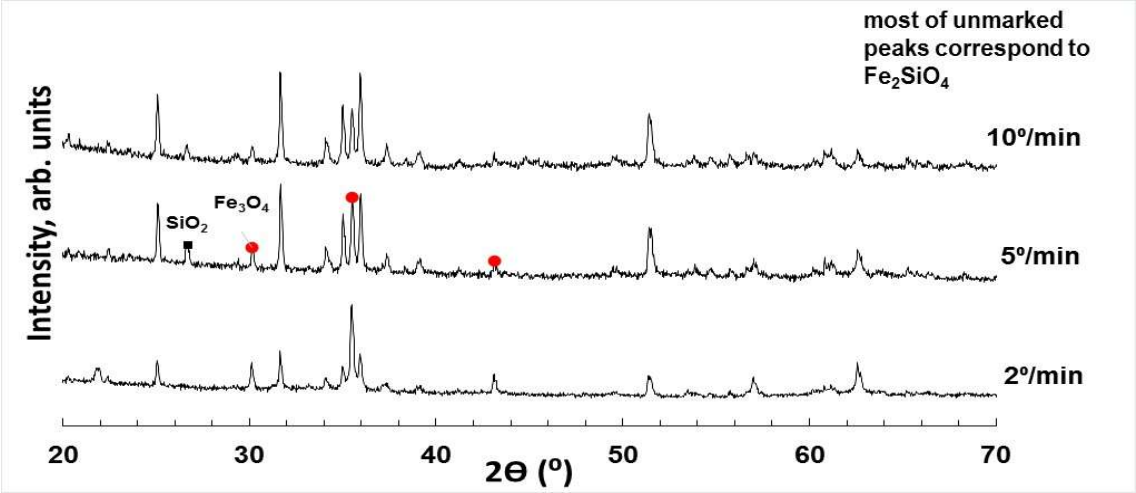

Fig. 22: XRD patterns of powdered samples (SiC+Fe_2O_3) after heating/cooling cycle in dry CO_2 to 1100°C with different rates. Pre-treatment: ball-milling at 150 rpm for 4h. Initial sample weight ≈0.3 g.

Pelletized samples offer better conditions to promote formation of Fe_2SiO_4 and also to prevent undue oxidation (Fig.23). One may assume that intimate contact of reactants promotes reactivity between SiC and Fe_2O_3, and that the limited porosity of pelletized samples offer best conditions to control the supply of additional oxygen by limiting the access of CO_2, thus preventing subsequent oxidation of Fe_2SiO_4 to silica, and even minimizing the onset of magnetite for sufficiently fast cycles. Thus, comparative studies of reactivity

in powdered (Fig.22) and pelletized (Fig.23) samples emphasized the importance of kinetic factor in formation of Fe_2SiO_4 preventing further oxidation to Fe_3O_4 and SiO_2.

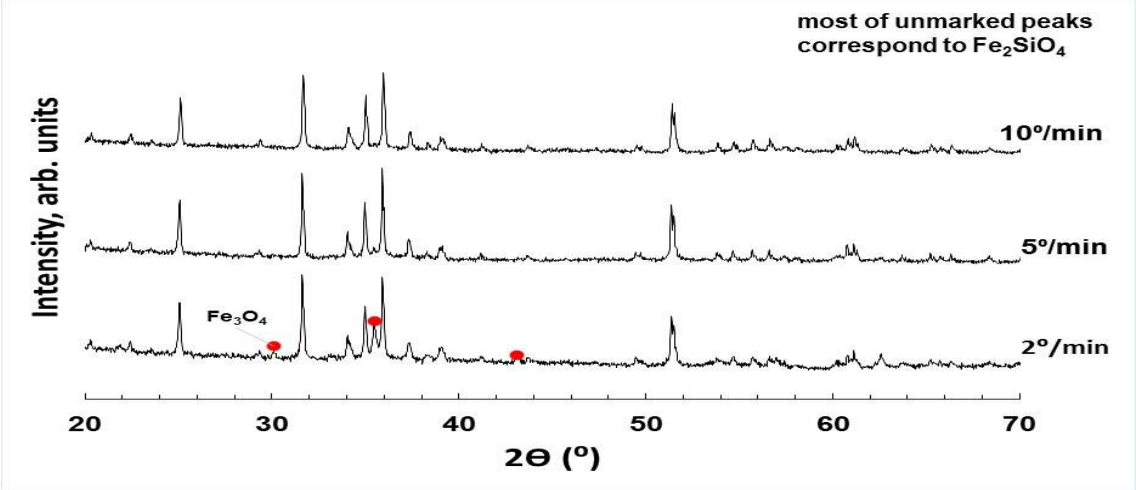

Fig. 23: XRD patterns of pelletized samples ($SiC+Fe_2O_3$) after hating/cooling cycle in dry CO_2 to 1100°C with different rates. Pre-treatment: ball-miling at 150 rpm for 4h. Initial sample weight ≈0.3 g.

High-energy milling of the initial reagents mixture yields finer grain sizes, and possibly even amorphisation of precursor powders, thus yielding conditions for an initial stage of high reactivity between SiC and Fe_2O_3, without passivation. By shortening the initial stage one also expects limited contribution of CO_2 (as a supplementary oxidant) and this oxygen shortage maintains highly reducing conditions and, thus, significant fractions metallic Fe, mainly for the shortest cycles (Fig.24). In this case, one may also assume that magnetite is formed by subsequent oxidation of metallic Fe, as indicated by the dependence on heating rate.

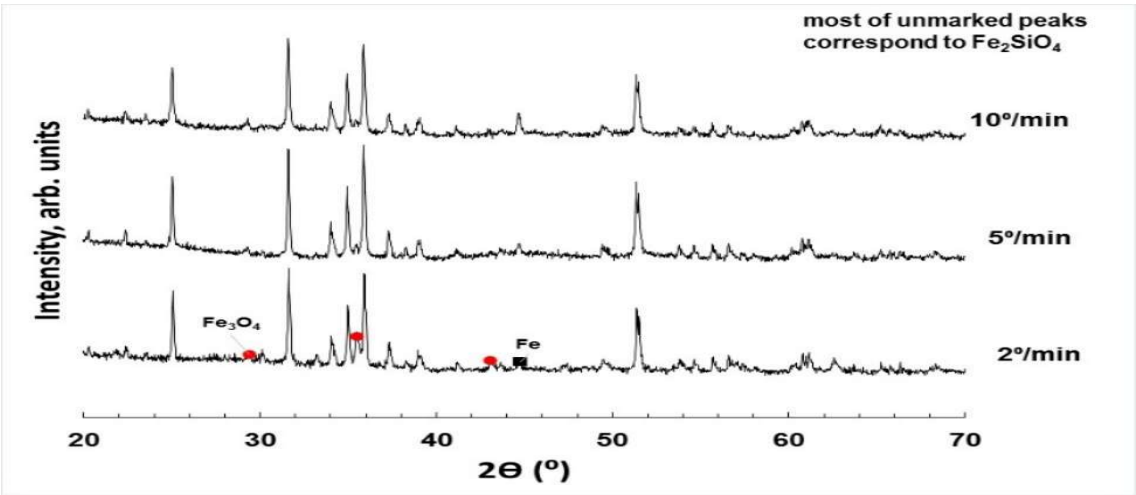

Fig. 24: XRD patterns of pelletized samples ($SiC+Fe_2O_3$) after heating/cooling cycle in dry CO_2 to 1100°C with different rates. Pre-treatment: high-energy milling at 600 rpm for 4h. Initial sample weight ≈0.3 g.

Thus, the best selected conditions for Fe_2SiO_4 formation correspond to thermal treatment of pelletized samples in dry CO_2 flow with a highest heating/cooling rate and minimum treatment at 1100ºC.

3.2.5 Final preparation of Fe_2SiO_4 samples for preliminary catalyst testing

The initial studies of catalyst synthesis were performed with smaller pelletized samples (~ 0.3 g), and catalyst testing in real biomass gasification conditions requires upscaling by at least two orders of magnitude. Thus, one needed to revise the preparation procedures. The initial attempts showed greater difficulties than found for small samples, namely because evolution of large quantities of gases (CO_2+CO) as reaction products from oxidation of SiC resulted in highly foamed samples, which were prone to undergo oxidation to unwanted silica and magnetite (Fig.25 B and C, as opposed to A). This may be ascribed to difficulties in preventing subsequent oxidation of the fayalite phase at the latest stages of processing.

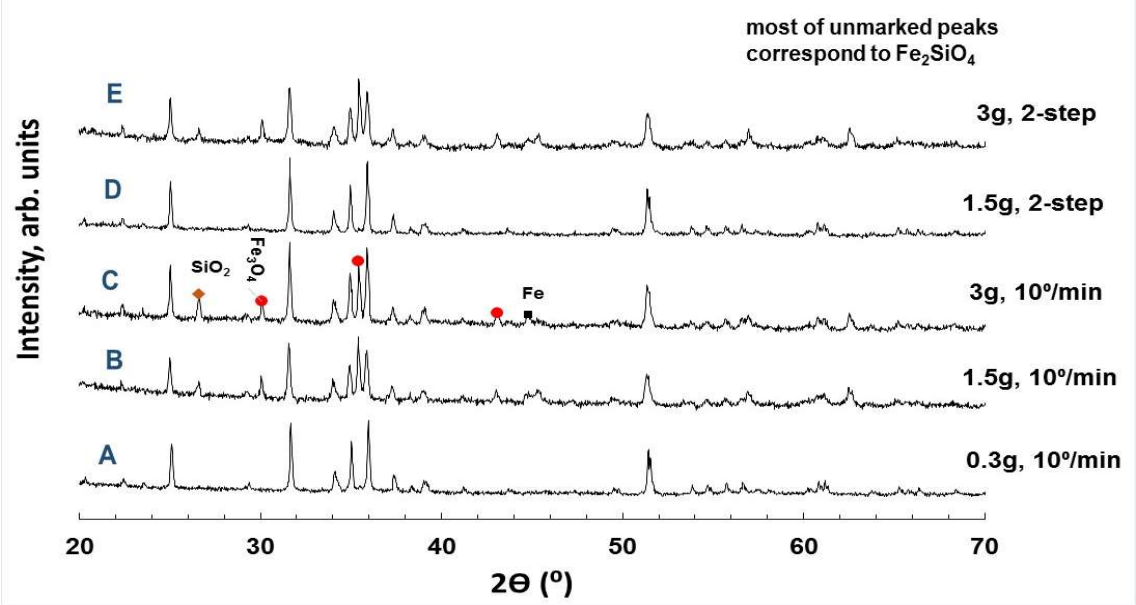

Fig. 25: XRD patterns of pelletized samples (SiC+Fe_2O_3) of different mass after heating/cooling cycle in dry CO2 to 1100°C with different heating profiles. The first heating profile is a simple heating/cooling cycle at 10°C/min. 2-step thermal treatment profile is shown in Fig. 27.

The firing procedure was therefore modified based on guidelines provided by thermogravimetry; this was performed by TGA studies comprising an initial stage on heating at constant rate and then an isothermal plateau at the peak temperature of 1100ºC, based on the above described synthesis studies. Thus, one could monitor the relevant steps of SiC oxidation upon heating SiC+Fe_2O_3 mixture in CO_2 flow (Fig.26), which comprises the initial stage with gradual weight losses, and then sharp evolution of gases at ~910ºC, as indicated by a mass drop. This is followed by a weight gain due to oxidation of powdered precursor mixture.

The final firing profile for larger pelletized samples was change therefore to include 2-step heating (Fig. 27): slower until 980ºC to account for gas release and prevent foaming, and faster at higher temperatures to prevent undesired overoxidation.

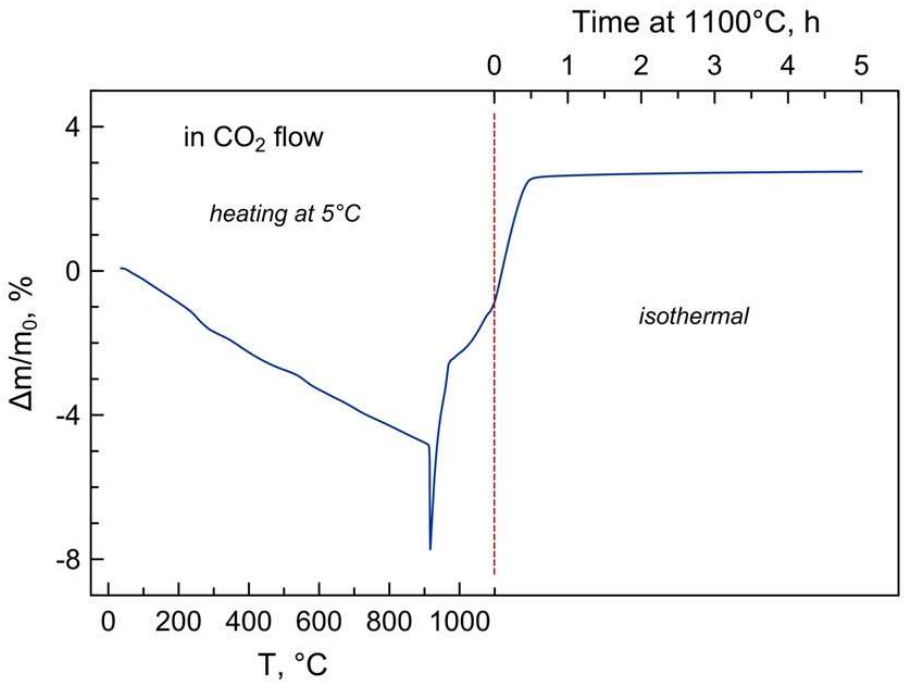

Fig. 26: Thermogravimetric curve of powdered Fe_2O_3+SiC sample on heating at 5°C/min for up to 1100ºC, and subsequent isothermal treatment at 1100ºC, in dry CO_2 flow.

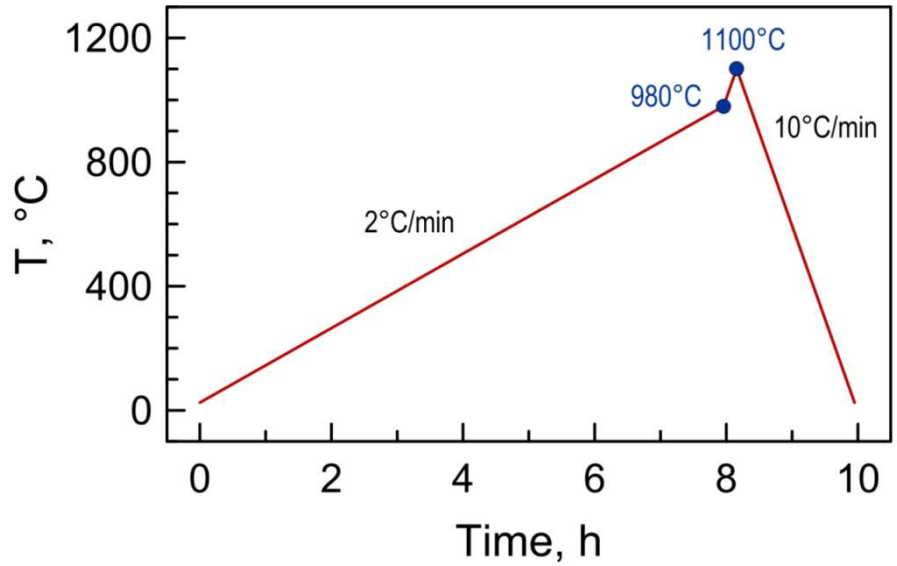

Fig. 27: Final firing profile with 2-step heating.

With modified firing profile, the release of gas is still too extensive for 3 g pellets resulting again in a foaming (Fig. 28A and 29A) and formation of unwanted SiO_2 and Fe_3O_4 (Fig.25 E). At the same time, firing of 1.5 g samples yielded porous pellets (Fig.28 B and 29 B) comprising phase-pure Fe_2SiO_4 phase (Fig.30). Thus, this procedure was selected for larger-scale preparation of synthetic fayalite for the scheduled catalytic tests.

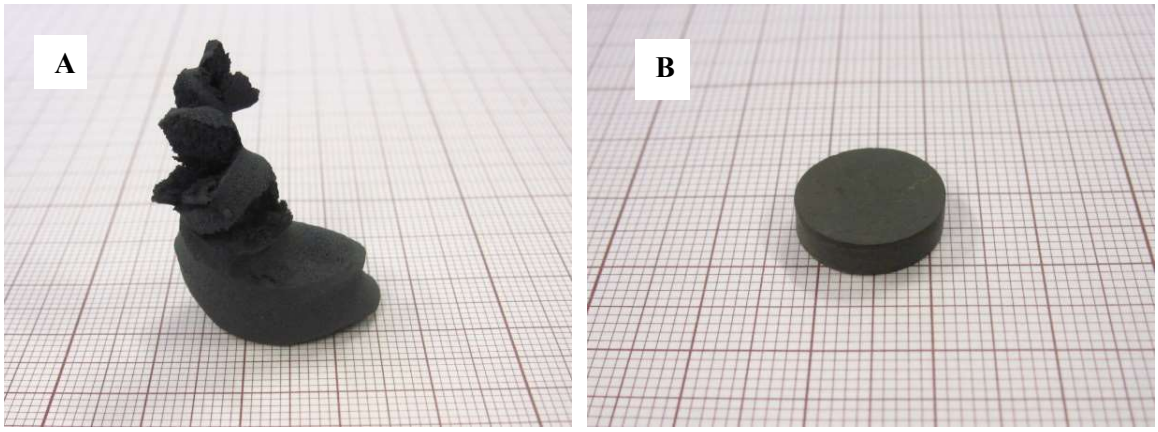

Fig. 28: Images of 3 g (A) and 1.5 g (B) pellets obtained using final 2-step firing profile.

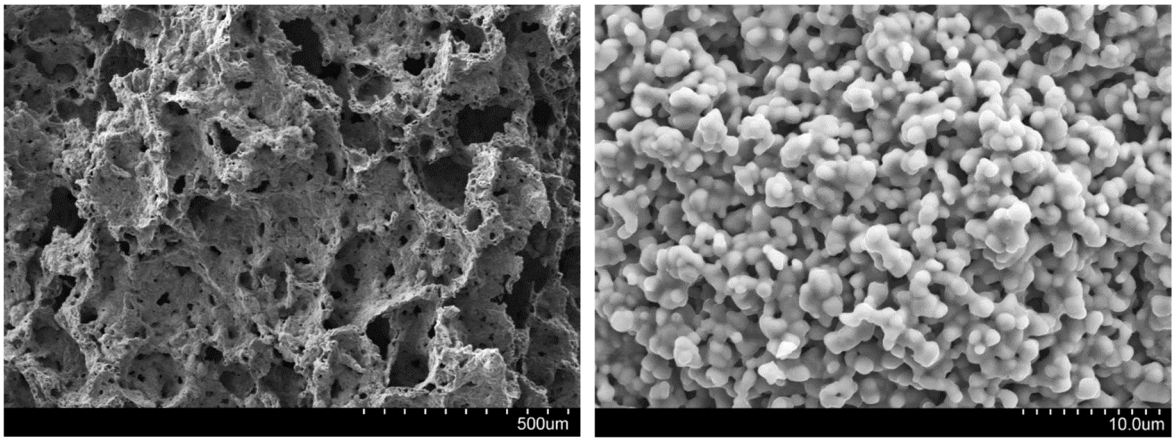

Fig. 29: SEM micrographs of 3 g foamed multiphase sample containing Fe_2SiO_4 + SiO_2 +Fe_3O_4 (left) and a porous single phase Fe_2SiO_4 samples (right).

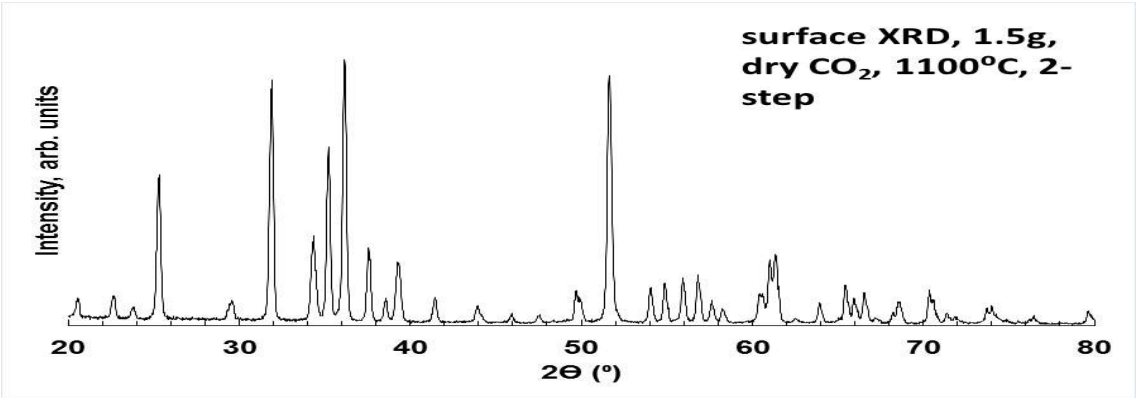

Fig. 30: XRD pattern of the final product showing pure fayalite phase

3.3 Catalytic test in bed-fluidized reactor

For the test of catalytic activity, 26 g of powdered fayalite catalyst were distributed in 3 tiers in sample holder (Fig.14). The gasification tests (0 % of O_2) were conducted comparatively for 1 h with catalyst and 1 h without catalyst.

Ceramic fibre (ceramic blanket) was used to separate catalyst layers, Fig 31; this as also used as a marker for deposition of carbon after gasification.

The condensation of tar was clearly visible in a bubbler at the outlet of reactor during the experiment without the catalyst (Fig. 32, left), while no presence of tar was observed after the experiment with Fe_2SiO_4 as catalyst (Fig. 32, right)

Fig. 31: Ceramic blanket before (left) and after (right) the catalytic test.

Fig. 32: Example of impingers used for tar condensation at the outlet of the reactor, showing condensation of tar in the biomass gasification experiment without catalyst (a) and low content of tars in experiment with Fe_2SiO_4 catalyst (b).

The results of chromatographic gas analyses from gasification reactors with and without catalyst are listed in Table 10. CO_2 (and apparently, H_2O) were the main products in experiment without catalyst, combined with non-negligible fractions of light hydrocarbons (CH_4, C_2H_4, …). One the contrary, the use of Fe_2SiO_4 catalyst promoted prevailing partial oxidised CO and enhanced the fraction of H_2, while eliminating traces of hydrocarbons. These trends suggest that the mechanisms assisted by Fe_2SiO_4 catalysts may include promotion of CO_2 reforming and/or steam reforming reactions. However, this is just a preliminary screening of catalyst activity and a detailed study of mechanisms is beyond the scope of this MSc thesis.

Table 10: Composition of gasification product.

[%, v/v dry gas]	Without catalyst	With catalyst (first 5 min.)	With catalyst
CH_4	2.0	0.0	0.0
CO	9.3	34.2	37.6
CO_2	11.6	6.6	3.6
C_2H_4	0.7	0.0	0.0
C_2H_6	0.1	0.0	0.0
C_3H_8	0.03	0.00	0.00
H_2	4.8	12.9	14.7
N_2 (by diference)	71.5	46.2	44.0

XRD was also used for post-mortem inspection of the catalyst after catalytic experiment; this is shown in Fig.33, and demonstrates that Fe_2SiO_4 phase is still retained as a major phase, although operation under conditions of tar conversion and producer gas upgrading resulted in partial reduction with clear evidence of formation of metallic Fe, possibly combined with segregation of silica. However, one must emphasize that the body-centered cubic (bcc) structure of metallic Fe yields very intense XRD reflections. Thus, the relative fraction of metallic Fe must be much smaller than suggested by the relative intensity of the Fe reflection in Fig.33. Detailed studies of long term testing are also beyond the scope of the MSc thesis and require subsequent work.

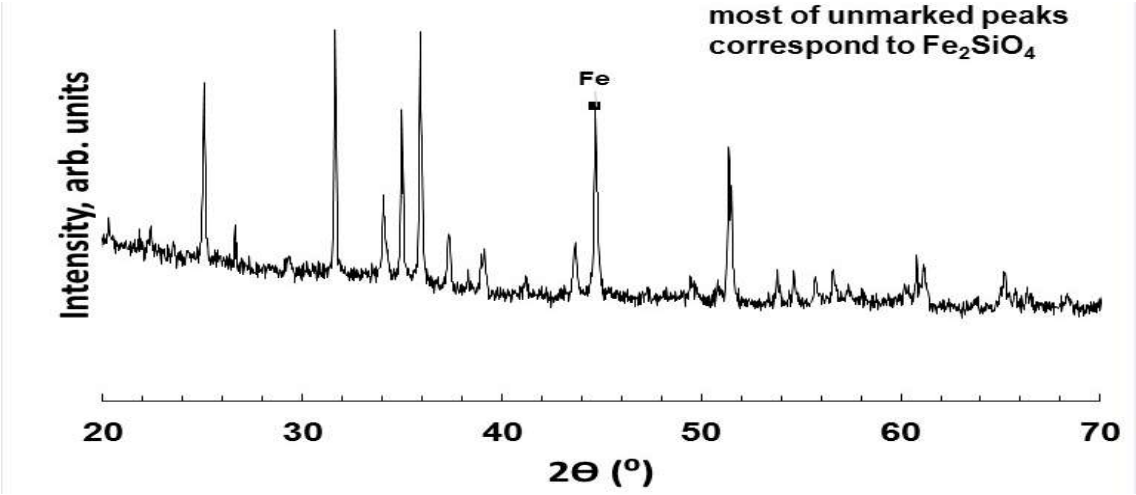

Fig. 33: XRD pattern of Fe_2SiO_4 catalyst after catalytic tests.

3.4 Attempts of preparation of Fe_2SiO_4/SiC core-shell catalyst

The final objective was intented to demonstrate the hypothesis of developing SiC/Fe_2SiO_4 core-shell catalysts, with ability to combine the catalytic properties of Fe_2SiO_4 with self-heating by microwave absorption, relying on the SiC core; this is expected to promote endothermic reactions such as reforming.

For this one tried different alternatives with SiC (fine) and SiC (coarse grained) mixing with ethanol iron nitrate, iron oxalate and hematite. Fig 34 shows the schematic procedure for reaction of SiC with iron nitrate and iron oxalate.

In the beginning, one used iron nitrate or iron oxalate (Fig. 35 to Fig. 37), and different combinations of temperatures (850 ºC – 1100 ºC) and times (2, 5 and 10 h). These attempts failed to yield Fe_2SiO_4, except for traces, and the main reaction products were magnetite, hematite, silica, combined with the 6H-SiC moissanite phase. Though this shows that the coarse silicon carbide cores are retained, this procedure failed to promote Fe_2SiO_4 by reaction between fine SiC and the Fe-precursors, yielding mainly separate oxidized phases, i.e. SiO_2 and $Fe_2O_3 + Fe_3O_4$.~

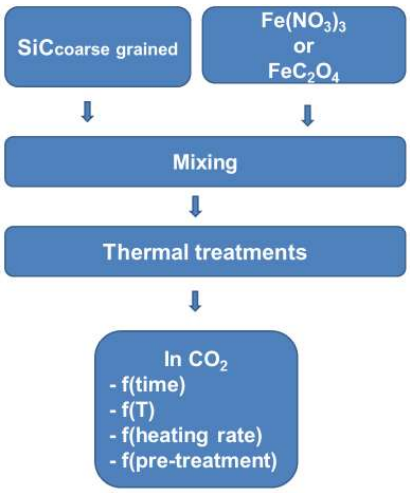

Fig. 34: Schematic representation for the first attempts to prepare core-shell catalysts.

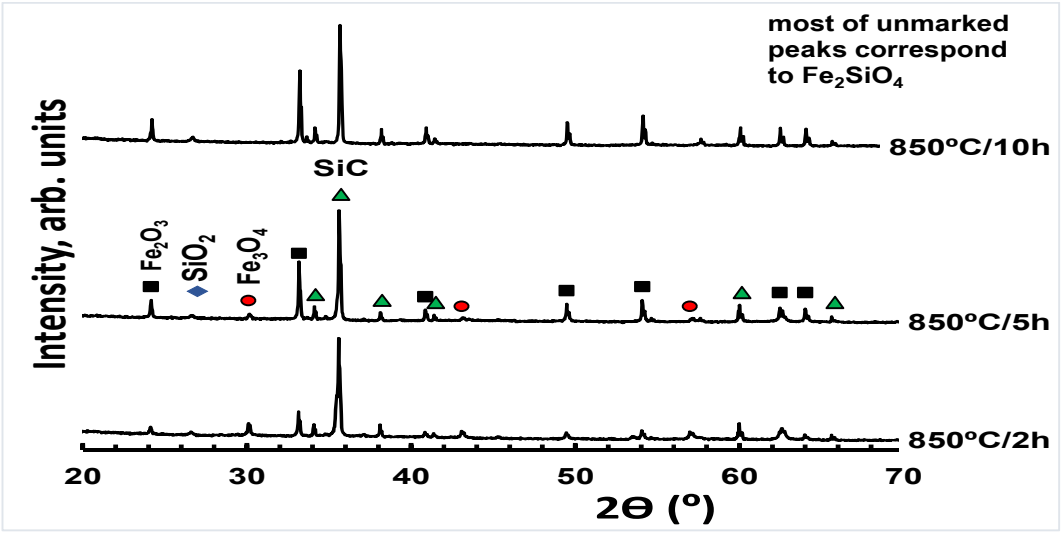

Fig. 35: XRD patterns of powdered samples ($SiC+FeC_2O_4*2H_2O$) after treatment in dry CO_2 flow at 850°C for different time. Initial sample weight ≈0.3 g

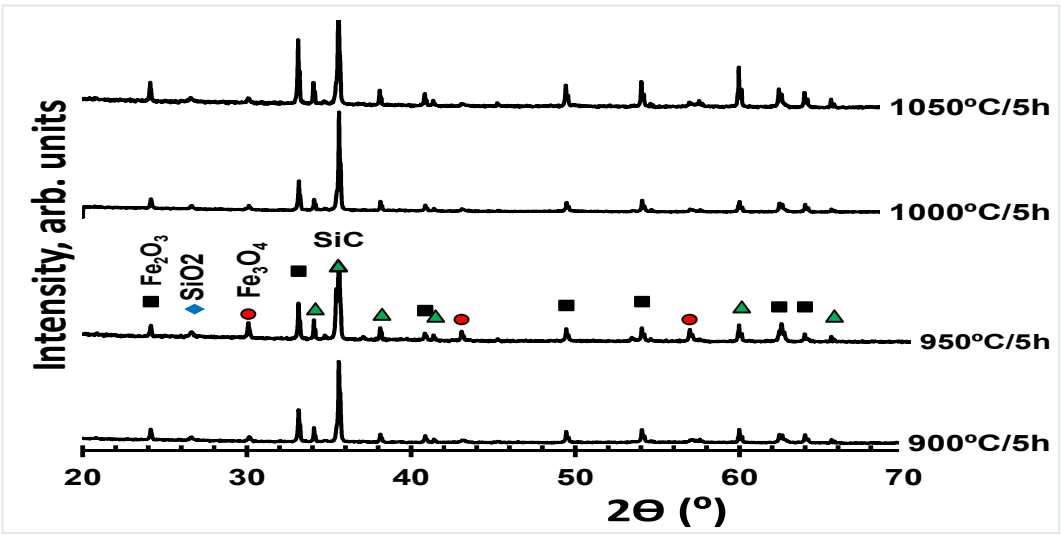

Fig. 36: XRD patterns of powder samples ($SiC+FeC_2O_4*2H_2O$) after treatment in dry CO_2 flow for 5 h at 900°C to 1050°C. Initial sample weight ≈0.3 g

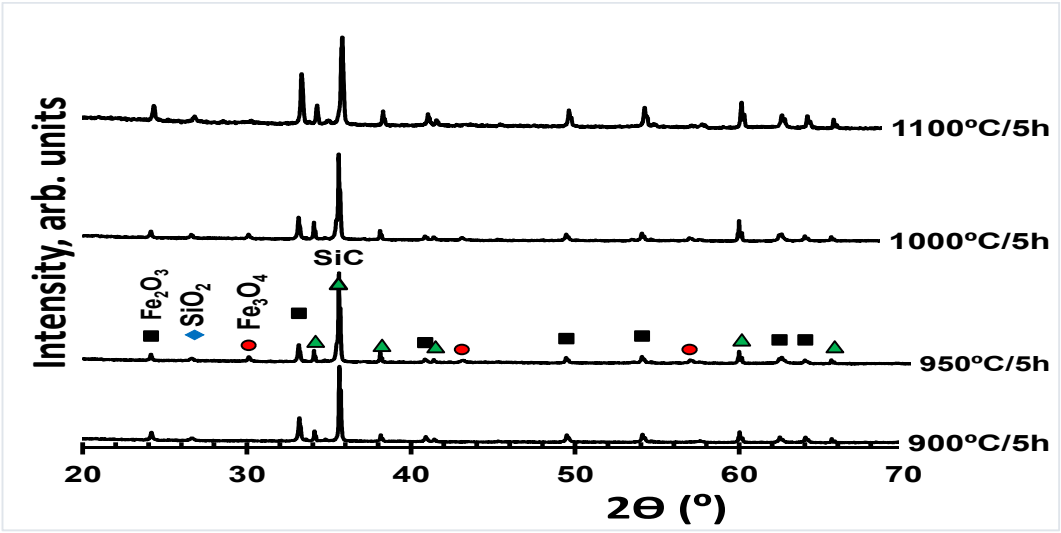

Fig. 37: XRD patterns of powder samples (SiC+$Fe(NO_3)_3$*$9H_2O$) after treatment in dry CO_2 flow for 5 h at 900°C to 1100°C

The next procedure relied on a mixture of hematite with fine SiC. Terpinol was then added to this mixture, to form a slurry, and coarse SiC particles were then added to that slurry, as described in Fig. 38. This procedure was partially successful, yielding Fe_2SiO_4 combined with the main reflections of SiC core particles. Minor contents of SiO_2 and traces of Fe_3O_4 are also shown, indicating that the firing schedule may still require optimization (Fig. 39). Nevertheless, one may conclude that this approach is feasible to process core-shell SiC-Fe_2SiO_4 catalysts.

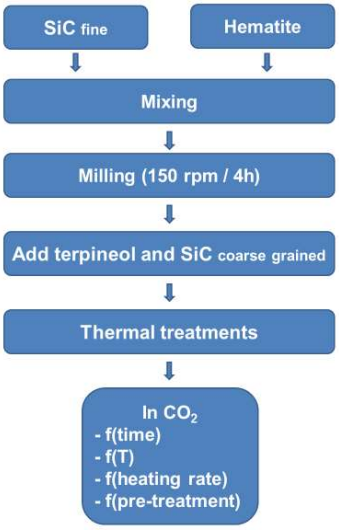

Fig. 38: Final procedure for synthesis of core-shell catalyst

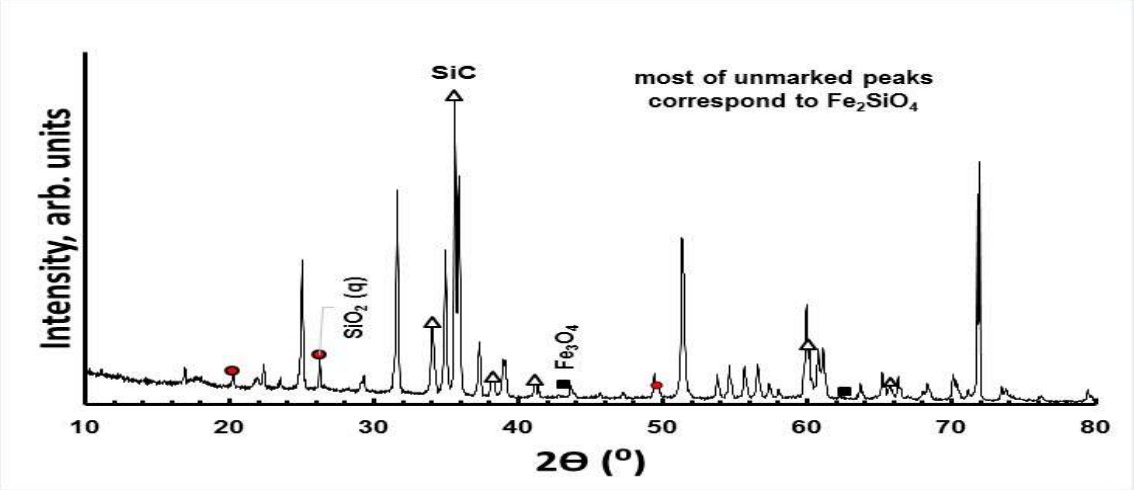

Fig. 39: XRD patterns of powder samples ($SiC+Fe_2O_3$) after treatment in dry CO_2 flow for 5 h at 1100°C

IV. Conclusion

Fayalite Fe_2SiO_4 was synthesized as a tar removal catalyst by reaction of stoichiometric mixture of Fe_2O_3:SiC = 1:1, in controlled atmospheres at 1000-1100 ^{0}C. Thermodynamic predictions provide guidelines for suitable redox conditions to synthesize Fe_2SiO_4. However, this was also found dependent on key kinetic limitations and related factors were identified. The first critical factor was to find a required oxygen supply to compensate for the unbalanced O:Fe:Si:C ratios in the reactants. One attempted to adjust this was the supply of humidified Ar, based on the expected ability of the H_2O/H_2 pair to adjust suitable redox conditions. However, this did not allow suitable conditions to overcome onset of undesired oxidised phases, co-existing with metallic Fe as a major phase. This may be ascribed to the high reactivity of steam with SiC, yielding SiO_2 even under oxygen deficient conditions, as revealed by simultaneous onset of metallic Fe as a major phase. The redox stability of SiO_2 prevents its subsequent reactivity, even in the presence of metallic Fe.

The alternative CO_2 flow offers best prospects to adjust the required redox conditions and is less reactivity with SiC. Thus, this allows preferential reactivity of SiC with Fe_2O_3, yielding Fe_2SiO_4, rather than direct reaction with the oxidant (CO_2) and onset of the unwanted SiO_2 phase. TGA confirmed ability to de-convolute the relevant intermediate steps, and also gave guidelines to prevent subsequent oxidation to SiO_2 and/or Fe_3O_4, by controlling the firing schedule, i.e., the upper temperature and heating rate or dwell time. Note that longer firing schedules imply risks of excessive oxygen supply by the CO_2 flow and, thus, risks of onset of unwanted oxidised phases, mainly at the highest temperatures.

Other factors such as state of compaction of reactants mixtures, and size of compacted pellets also confirm the role of kinetics; this is understood by taking into account that compaction promotes best contact between the solid reactants ($SiC+Fe_2O_3$) and ensures slower supply of the oxidising gases. Still, this may be countered by the expansive evolution of large volumes of gases ($CO+CO_2$). High energy milling also promotes faster reactivity, and additional difficulties in preventing onset of unwanted phases.

Preliminary testing of Fe_2SiO_4 catalysts demonstrated their activity to upgrade producer gas obtained by gasification of biomass. In addition to the decrease in the content of condensable tars in the raw gas, the catalyst lowered the residual contents of light hydrocarbons (e.g., CH_4), and also lowered the contents of fully oxidised gases (CO_2 and H_2O), possibly suggesting that Fe_2SiO_4 catalyses reforming reactions, and promotes an increase in the concentration of CO and H_2.

Attempts to develop a suitable method for core-shell SiC-Fe_2SiO_4 catalysts also emphasize the issues of kinetics. One attempted to retain a stable SiC core by providing the excess of SiC as a fraction of coarse SiC particles (≈0,1 mm), while finer SiC particles (in the μm range) were used to promote reactivity with Fe precursor to synthesize the intended Fe_2SiO_4 shell. Initial attempts based on Fe-precursors added as aqueous solutions of Fe precursors failed, probably because these were based on Fe-nitrate or oxalate. These failures may be understood by taking into account their early decomposition and the high reactivity of SiC with wet oxidising atmospheres.

Much better results were obtained by impregnating the coarse SiC particles with suspensions of fine SiC+Fe_2O_3 powder mixtures and then firing under CO_2 flow; this provides convincing guidelines for future optimization of a feasible processing method for core-shell SiC-Fe_2SiO_4 catalysts.

Bibliography

[1] L. Devi, M. Craje, P. Thune, K. J. Ptasinski and FransJ.J.G.Janssen, "Olivine as tar removal catalyst for biomass gasifiers: Catalyst characterization," *Applied Catalysis,* vol. 294, pp. 68-79, 2005.

[2] V. Claude, C. Courson, M. Kohler and S. D. Lambert, "Overview and Essential of Biomass Gasification Technologies and Their Catalytic Cleaning Methods," *energy&fuels,* vol. 30, pp. 8791-8814, 2016.

[3] D. Swierczynski, S. Libs, C.Courson and A. Kiennemann, "Steam reformin of tar from a biomass gasification process over Ni/olivine catalyst using toluene as a model compound," *Applied Catalysis,* vol. 74, pp. 211-222, 2007.

[4] A. Hussain, S. M. Arif and M. Aslam, "Emerging renewable and sustainable energy technologies: State of the art," *Renewable and Sustainable Energy Reviews,* pp. 12-28, 08 Jannuary 2017.

[5] Eurostat, "Share of renewables in energy consuption in the EU still on the rise to almost 17% in 2015," *Eurostat NewsRelease,* p. 3, 2017.

[6] L. Nunes, J. Matias and J.P.S.Catalão, "Biomass in the generation of electricity in Portugal: A review," *Renewable and Sustainable Energy Reviews,* vol. 71, pp. 373-378, 2016.

[7] W. M. K. D. P. J. P. M. R. B. S. Haris Doukas, "A methodology for validating the renewable energy data in EU," *Renewable Energy,* pp. 1981-1998, 2006 December 2007.

[8] Eurostat, "The contribution of renewable energy up to 12.4% of energy consumption in the EU27 in 2010," *Eurostat newsrelease,* p. 2, 2012.

[9] Eurostat, "Share of renewables in energy consumption up to 14% in 2012," *Eurostat newsrelease,* p. 3, 2014.

[10] Eurostat, "Share of renewables in nergy consumption up to 15% in the EU in 2013," *Eurostat newsrelease,* p. 4, 2015.

[11] P. McKendry, "Energy production from biomass (part 1): overview of biomass," *Bioresource Technology,* vol. 83, pp. 37-46, 2001.

[12] F. Frombo, R. Minciardi, M. Robba, F. Rosso and R. Sacile, "Planning woody biomass logistics for energu production: A strategic decision model," *Biomass & Bioenergy,* vol. 33, pp. 372-383, 2009.

[13] Y. Shen, X. G. Junfeng Wang and M. Chen, "By-products recycling for syngas cleanup in biomass pyrolysis - An overview," *Renewable and Sustainable Energy Reviews,* vol. 59, pp. 1246-1268, 2016.

[14] Y. Shen and K. Yoshikawa, "Recent progresses in catalytic tar elimination during biomass gasification or pyrolysis - A review," *Renewable and Sustainable Energy Reviews,* vol. 21, pp. 371-392, 2013.

[15] L. Devi, K. J. Ptasinski, F. J. G. Janssen, S. V. v. Paasen, P. C.A.Bergman and J. H. Kiel, "Catalytic decomposition of biomass tars: use of dolomite and untreated olivine," *Renewable Energy,* vol. 30, pp. 565-587, 2005.

[16] L. Devi, K. J. Ptasinski and F. J.J.G.Janssen, “A review of the primary measures for tar elimination in biomass gasification processes,” *Biomass & Bioenergy,* vol. 24, pp. 125-140, 2003.

[17] Z. A. El-Rub, E. A. Bramer and G.Brem, “Review of Catalysts for Tar Elimination in Biomass Gasification Processes,” *Ind. Eng. Chem. Res.,* vol. 43, pp. 6911-6919, 2004.

[18] S. Anis and Z. Zainal, “Tar reduction in biomass producer gas via mechanival, catalytic and thermal methods: A review,” *Renewable and Sustainable Energy Reviews,* vol. 15, pp. 2355-2377, 2011.

[19] D. Swierczynski, C. Courson, L. Bedel, A. Kiennemann and S.Vilminot, “Oxidation Reduction Behavior of Iron-Bearing Olivines (FexMg1-x)2SiO4 Used as Catalysts for Biomass Gasification,” *Chem. Mater,* vol. 18, pp. 897-905, 2006.

[20] L. Devi, M. Craje, P. Thune, K. J. Ptasinski and F. J. Janssen, “Olivine as tar removal catalyst for biomass gasifiers: Catalyst characterization,” *Applied Catalyst,* vol. 294, pp. 68-79, 2005.

[21] J. N. Kuhn, Z. Zhao, L. G. Felix, R. B. Slimane, C. W. Choi and U. S. Ozkan, “Olivine catalysts for methane- and tar-steam reforming,” *Applied Catalysis,* vol. 81, pp. 14-26, 2008.

[22] V. Meynen, P. Cool and E. Vansant, “Verified syntheses of mesoporous materials,” *MIcroporous and Mesoporous Materials,* vol. 125, pp. 170-223, 2009.

[23] M. E. Brown, Handbook of thermal analysis and calorimetry, Sara Burgerhartstraat 25: Amsterdam, The Netherlands, 1998.

[24] D. Pio, L. Tarelho and M. Matos, “Characteristics of the gas produced during biomass direct gasification in an autothermal pilot-scale bubbling fluidized bed reactor,” *Energy,* vol. 120, pp. 915-928, 2017.

[25] H. Yokokawa, N. Sakai, T. Kawada and M. Dokiya, “Thermodynamic stability of perovskites and related compounds in some alkaline earth-transition metal-oxygen systems,” *Journal of Solid State Chemistry,* vol. 94, pp. 106-120, 1991.

[26] J. Monteiro, “Chemical potential diagrams as guideline for phase stability and reactivity of cementitious systems, MSc Thesis,” Universidade de Aveiro, 2009.

[27] C. W. Bale, A.D.Pelton, W. Thompson, G. Eriksson, K. Hack, S. D. P. Chartrand and J. Melacon, “FactSage 5.5, Thermfact and GTT-Technologies,” 1976-2007.

[28] M. Jacobs, B. D. Jong and H. Oonk, “The Gibbs energy formulation of alpha, gamma, and liquid Fe2SiO4 using Grover, Getting and Kennedy's empirical relation between volume and bulk modulus,” *Geochimica et Cosmochimica Acta,* vol. 65, pp. 4231-4242, 2001.

[29] E. Opila, “Variation of the oxidation rate of silicon carbide with water-vapor-pressure,” *J. Amer. Ceram. Soc.,* vol. 82, pp. 625-636, 1999.

[30] Q. N. E.J.Opila, “Oxidation of chemically-vapor-depositedsilicon carbide in carbon dioxide,” *J. Amer. Ceram. Soc.,* vol. 81, pp. 1949-1952, 1998.

[31] J. Roy, S. Chandra, S. Das and S. Maitra, “Oxidation behaviour of silicon carbide - A review,” *Reviews on advanced materials science,* vol. 38, pp. 29-30, 2014.

[32] G. Renlund, S. Prochazka and R.H.Doremus, “Silicon oxycarbide glasses. 2-structure and properties,” *Journal of Material Research,* vol. 6, pp. 2723-2734, 1991.